Article

Immunoglobulin M perception by FcμR

Yaxin Li[1,5], Hao Shen[1,5], Ruixue Zhang[2,5], Chenggong Ji[1], Yuxin Wang[1], Chen Su[1] & Junyu Xiao[1,3,4 ✉]

Immunoglobulin M (IgM) is the first antibody to emerge during embryonic development and the humoral immune response[1]. IgM can exist in several distinct forms, including monomeric, membrane-bound IgM within the B cell receptor (BCR) complex, pentameric and hexameric IgM in serum and secretory IgM on the mucosal surface. FcμR, the only IgM-specific receptor in mammals, recognizes different forms of IgM to regulate diverse immune responses[2–5]. However, the underlying molecular mechanisms remain unknown. Here we delineate the structural basis of the FcμR–IgM interaction by crystallography and cryo-electron microscopy. We show that two FcμR molecules interact with a Fcμ-Cμ4 dimer, suggesting that FcμR can bind to membrane-bound IgM with a 2:1 stoichiometry. Further analyses reveal that FcμR-binding sites are accessible in the context of IgM BCR. By contrast, pentameric IgM can recruit four FcμR molecules to bind on the same side and thereby facilitate the formation of an FcμR oligomer. One of these FcμR molecules occupies the binding site of the secretory component. Nevertheless, four FcμR molecules bind to the other side of secretory component-containing secretory IgM, consistent with the function of FcμR in the retrotransport of secretory IgM. These results reveal intricate mechanisms of IgM perception by FcμR.

IgM serves as the first line of defence against infections in humoral immunity. The predominant form of IgM in serum is a pentameric assembly (pIgM), with five IgM monomers joined together by the joining chain (J-chain). In the absence of the J-chain, hexameric IgM can be formed. The Fc tailpiece has a vital role in IgM polymer formation and J-chain incorporation. In addition to functioning in polymeric antibody forms, the monomeric membrane-bound IgM (mIgM) participates in the BCR complex, together with Igα (also known as CD79A) and Igβ (also known as CD79B), and has a key role in antigen recognition and B cell activation. A transmembrane segment is present in mIgM for membrane localization in place of the tailpiece.

Different immunoglobulin classes feature different Fc regions, which are recognized by specific Fc receptors to elicit distinct effector mechanisms. For example, polymeric immunoglobulin receptor (pIgR) selectively recognizes J-chain-containing pIgM[6,7], as well as J-chain-containing dimeric, tetrameric or pentameric IgA[8,9], and escorts them to the mucosal surface. The ectodomain of pIgR, known as the secretory component (SC), remains bound to pIgM, resulting in the formation of the secretory IgM (sIgM) complex[10]. Two other IgM Fc (Fcμ) receptors are present in humans in addition to pIgR: FcαμR and FcμR[11]. FcαμR is involved in the internalization of IgM-coated microorganisms[12], and similar to pIgR, FcαμR binds both IgM and IgA. By contrast, FcμR binds IgM exclusively and is the only IgM-specific receptor in mammals.

Previously known as Toso or Faim3, FcμR was first identified as an inhibitor of Fas-mediated apoptosis in T cells[13] before it was demonstrated to be the long-sought Fc receptor for IgM[2,14]. *Fcmr*-knockout mice produce a myriad of phenotypes, suggesting that FcμR has critical functions in B cell development and immune tolerance[4,15–21]. FcμR is also involved in T cell activation[22] and T helper 17 cell pathogenicity[23]. In addition to these lymphocyte-related functions, FcμR has also been implicated in the activation of myeloid cells and their responses to cancer[24–26], although this functional aspect is under debate[27,28]. In addition, FcμR participates in mucosal immunity by mediating the retrotransport of sIgM–antigen complexes back from the mucosa[5]. Of note, FcμR is highly expressed on chronic lymphocytic leukaemia B cells[2,29–32], and targeting FcμR using either an IgM–toxin conjugate[33] or engineered chimeric antigen receptor T cells[34] could provide new treatment strategies for chronic lymphocytic leukaemia.

FcμR interacts with all forms of IgM, including pentameric and hexameric IgM, as well as mIgM within the BCR[2–4,35]. It is involved in the internalization of soluble IgM–antigen complexes, but not the BCR, suggesting that it binds differently to polymeric and monomeric IgM[3,4,32]. Furthermore, as FcμR carries out the retrotransport of SC-containing sIgM[5], it can bind pIgM together with SC. Here we investigate the molecular mechanism of the FcμR–IgM interaction.

Crystal structure of FcμR-D1–Fcμ-Cμ4

The extracellular domain (ECD) of FcμR contains an immunoglobulin-like domain (D1) followed by an intrinsically disordered, highly O-linked glycosylated stalk region (Fig. 1a). We first present the crystal structure of FcμR-D1 in complex with the Fcμ-Cμ4 domain at 3.0 Å resolution (Fig. 1b and Extended Data Table 1). Surface plasmon resonance (SPR) experiments demonstrated that FcμR-D1 binds Fcμ-Cμ4 with high affinity, exhibiting a dissociation constant (K_d) value of approximately 3.2 nM

[1]State Key Laboratory of Protein and Plant Gene Research, School of Life Sciences, Peking University, Beijing, P. R. China. [2]Academy for Advanced Interdisciplinary Studies, Peking University, Beijing, P. R. China. [3]Peking-Tsinghua Center for Life Sciences, Peking University, Beijing, P. R. China. [4]Changping Laboratory, Beijing, P. R. China. [5]These authors contributed equally: Yaxin Li, Hao Shen, Ruixue Zhang. ✉e-mail: junyuxiao@pku.edu.cn
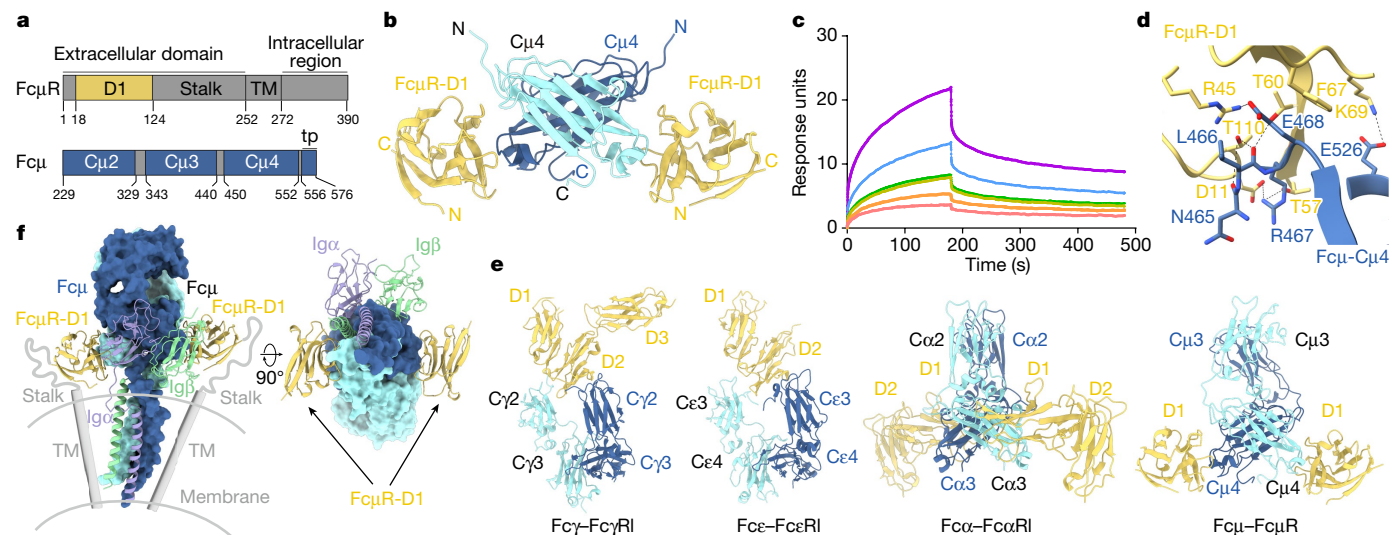
Fig. 1 | Crystal structure of the FcµR-D1–Fcµ-Cµ4 complex. a, Domain organizations of FcµR and Fcµ. TM, transmembrane; tp, tailpiece. **b**, Overall structure of the 2:1 FcµR-D1–Fcµ-Cµ4 complex. FcµR-D1 and Fcµ-Cµ4 are shown as ribbons, and the N and C termini of each molecule are indicated. **c**, SPR analyses of the FcµR-D1–Fcµ-Cµ4 interaction performed by passing twofold serial dilutions of purified Cµ4 (from 80 nM to 5 nM) to immobilized FcµR-D1. All SPR experiments in this paper were repeated at least two times. Fcµ-Cµ4 binding to FcµR-D1 $K_d = 3.17 \pm 0.63$ nM. **d**, The FcµR-D1–Fcµ-Cµ4 interface.

The dashed lines indicate polar interactions. **e**, Structural comparisons of the Fcγ–FcγRI (PDB ID: 4W4O), Fcε–FcεRI (PDB ID: 1F6A), Fcα–FcαRI (PDB ID: 1OW0) and Fcµ–FcµR complexes. The composite Fcµ–FcµR model was generated based on the FcµR-D1–Fcµ-Cµ4 crystal structure and the Fcµ structure (PDB ID: 6KXS). **f**, A composite model of two FcµR molecules bound to IgM BCR shown in two views. The model is generated by superimposing the structure of the FcµR-D1–Fcµ-Cµ4 complex onto that of IgM BCR (PDB ID: 7XQ8). The stalk and transmembrane regions of FcµR are sketched hypothetically.

(Fig. 1c and Extended Data Fig. 1). The structure reveals a 2:1 assembly, in which two FcµR-D1 molecules bind to an Fcµ-Cµ4 dimer from both sides. This is consistent with the previous finding that each IgM heavy chain contains an FcµR-binding site[36]. The interaction between FcµR-D1 and Fcµ-Cµ4 buries a surface area of 850 Å^2 and mainly focuses on the Fcµ-Cµ4 residues Asn465–Glu468 and Glu526 (Fig. 1d). Arg45$_{FcµR}$ from CDR-like loop 1 of FcµR forms an ion pair with Glu468. In CDR-like loop 2, Phe67$_{FcµR}$ packs against the aliphatic portion of Glu468, whereas Lys69$_{FcµR}$ coordinates Glu526. Thr110$_{FcµR}$ in CDR-like loop 3 forms hydrogen bonds with the main chain groups of Asn465 and Leu466, whereas Asp111$_{FcµR}$ interacts with Arg467. Thr57$_{FcµR}$ and Thr60$_{FcµR}$ from the C′ strand of FcµR also mediate hydrogen bond contacts with Leu466–Arg467. Asn465–Glu468 and Glu526 are uniquely present in Fcµ among the five classes of human immunoglobulins, which explains the specificity of FcµR for Fcµ (Extended Data Fig. 2a). A previous study has shown that the Q510R mutant of Fcµ abrogated the binding of FcµR-D1 (ref. [36]). In the structure, Gln510 is in close proximity to Lys73$_{FcµR}$; thus, the Q510R mutant may disrupt the binding via charge repulsion.

The binding mode between FcµR-D1 and Fcµ-Cµ4 is unique among the Fc–FcR complexes (Fig. 1e). The Fc receptors for IgG, including FcγRI (also known as CD64), FcγRII (also known as CD32) and FcγRIII (also known as CD16), form a 1:1 complex with Fcγ and bind to the lower hinge region on top of Cγ2 (ref. [37]). FcεRI, the receptor for IgE, binds Fcε in a similar manner[38]. By contrast, the IgA-specific receptor FcαRI (also known as CD89) forms a 2:1 complex with Fcα and targets the Cα2–Cα3 junction[39]. Here, FcµR also binds Fcµ with 2:1 stoichiometry; nonetheless, it interacts with the lower half of Cµ4 and approaches the Cµ4 dimer from a completely different angle.

The C termini of the two FcµR and two Fcµ molecules are located on the same side within the complex; thus, this structural arrangement would enable the interaction between FcµR and mIgM on the membrane. The long-awaited structure of IgM BCR has been recently unveiled[40–42]. Superimposing the structure of the FcµR-D1–Fcµ-Cµ4 complex onto that of IgM BCR revealed that the FcµR-binding site next to Igβ was completely exposed (Fig. 1f). The binding site next to Igα is also largely accessible, although an Asn97-glycan on Igα may slightly

interfere with the positioning of FcµR at this location. Indeed, FcµR co-precipitates with mIgM in the presence or absence of Igα and Igβ (Extended Data Fig. 1b), consistent with previous studies[3,4].

Cryo-EM structure of FcµR–Fcµ–J

Circulating IgM exists as both pentameric and hexameric assemblies, and a cell-based assay has suggested that FcµR can bind to both forms with nanomolar affinity or avidity[2,35]. Indeed, immobilized FcµR-D1 absorbs Fcµ–J, that is, the pentameric IgM core containing an Fcµ pentamer and the J-chain, with an apparent K_d of approximately 0.3 nM (Fig. 2a). The presence of antigen-binding fragments has no influence on this tight interaction, as FcµR-D1 binds to a recombinant full-length IgM (anti-CD20)[43] with similar affinity. To gain further insights into the structural basis of the FcµR–IgM interaction, we assembled a complex consisting of FcµR-ECD and Fcµ–J and performed cryo-electron microscopy (cryo-EM) analyses (Extended Data Table 2 and Extended Data Figs. 3 and 4). Both 1:1 and 4:1 FcµR–Fcµ–J complexes were observed in the cryo-EM data, and their structures were determined at resolutions of 3.4 Å and 3.7 Å, respectively.

In the 1:1 structure, a single FcµR occupies almost the same site on Fcµ–J as the D1 domain of SC in sIgM[6,7] (Fig. 2b). Similar to SC-D1, this FcµR-D1 interacts with multiple regions in Fcµ–J. First, it binds to the Cµ4 domain of Fcµ1B (the ten Fcµ chains in the Fcµ pentamer are labelled as previously described, with the Fcµ chain attached to the C-terminal hairpin of the J-chain as Fcµ1A[6]) in a similar manner to that seen in the crystal structure. There is still no contact between FcµR-D1 and the Cµ3 domains or the Cµ3–Cµ4 junctions. Second, Met42$_{FcµR}$–His43$_{FcµR}$ appears to pack on Tyr134$_J$ in the C-terminal region of the J-chain (Extended Data Fig. 4j). Last, Arg112$_{FcµR}$ contacts the tailpiece of Fcµ5B (Extended Data Fig. 4k). Together, this composite interface ensures the highly selective binding of FcµR-D1 at this site (R1 site).

In the 4:1 structure, four FcµR molecules are arranged into a semicircle (Fig. 2c). One of them binds at the R1 site, whereas the other three bind sequentially to Fcµ2–4 (R2–R4 sites). The binding of FcµR to Fcµ5 is prevented by the β2–β3 loop of the J-chain. At the R2–R4 sites, FcµR
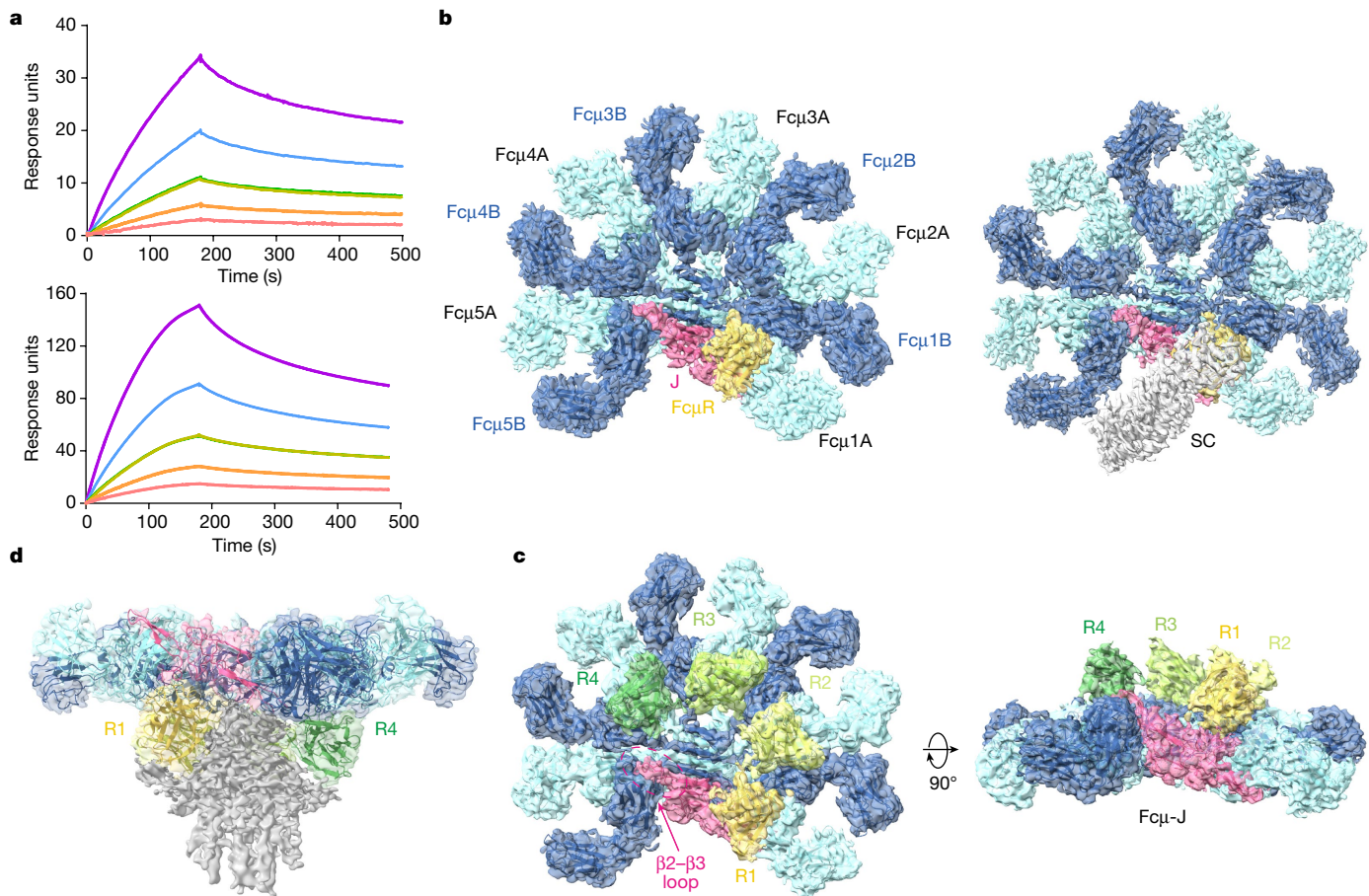
Fig. 2 | Cryo-EM structure of the FcµR-ECD–Fcµ–J complex. a, SPR analyses of the interactions between FcµR-D1 and Fcµ–J (top) or anti-CD20 IgM (bottom), performed by passing twofold serial dilutions of purified Fcµ–J or anti-CD20 IgM (both from 2 nM to 0.125 nM) to immobilized FcµR-D1. Fcµ–J binding to FcµR-D1 $K_d = 0.33 \pm 0.11$ nM, and anti-CD20 IgM binding to FcµR-D1 $K_d = 0.26 \pm 0.13$ nM. **b**, Overall structure of the 1:1 FcµR-ECD–Fcµ–J complex (left). The sIgM core structure is shown on the right for comparison. The Fcµ molecules are shown in two shades of blue, whereas the J-chain is shown in magenta. FcµR-D1 is shown in

yellow, so is the D1 domain of SC. The rest of SC is shown in white. **c**, Structure of the 4:1 FcµR-ECD–Fcµ–J complex shown in two views. The four FcµR molecules are shown in different shades of yellow and green and labelled R1–R4. The β2–β3 loop of the J-chain, which prevents the binding of FcµR to Fcµ5, is highlighted with a dashed circle. **d**, Unmodelled densities (grey) are present in the 4:1 FcµR-ECD–Fcµ–J complex, which most likely correspond to the stalk regions of the FcµR molecules.

docks onto the Cµ4 domains of Fcµ2B, Fcµ3B and Fcµ4B, as seen in the crystal structure. The C–C' loops of Fcµ1B-Cµ4, Fcµ2B-Cµ4 and Fcµ3B-Cµ4 from the adjoining Fcµ units also contribute to binding at these sites (Extended Data Fig. 4l). The four FcµR molecules all bind on the same side of Fcµ–J. This is in sharp contrast to the crystal structure, in which two FcµR molecules bind to both sides of the Cµ4 dimer. There is no notable contact among the four FcµR-D1 domains. Nevertheless, prominent densities are present within the FcµR-D1 semicircle and below the FcµR-D1 domains (Fig. 2d). These densities could not be unambiguously modelled but most likely belong to the stalk regions of FcµR, as the entire FcµR-ECD was used in the cryo-EM study. It is likely that the stalk regions bridge intermolecular interactions between the four FcµR molecules and facilitate their binding on the same side of Fcµ–J. This hypothesis is further supported by our observation that no 4:1 structure was visualized when FcµR-D1 was used to prepare the complex in place of FcµR-ECD, even when FcµR-D1 was present in 200-fold excess (Extended Data Fig. 5).

Cryo-EM structure of FcµR–Fcµ–J–SC

The fact that the R1 site overlaps with the binding site of SC-D1 raises the question of how FcµR enables the retrotransport of SC-containing

sIgM[5]. First, we confirmed that FcµR can indeed bind the core sIgM (Fcµ–J–SC) (Fig. 3a). Then, we determined the cryo-EM structure of FcµR in complex with Fcµ–J–SC at 3.2 Å (Extended Data Table 2 and Extended Data Fig. 6). We initially thought that FcµR might bind to the R2–R4 sites in this complex. To our surprise, four FcµR molecules instead bound to the opposite side of Fcµ–J (R1'–R4' sites; Fig. 3b). The binding environments at the R2'–R4' sites are highly similar to those of R2–R4. The R1' site is slightly different. In addition to mainly targeting Fcµ5A-Cµ4, R1' FcµR also contacts $Ser65_J$–$Asp66_J$ in the J-chain as well as Glu570 in the Fcµ1A tailpiece via $Arg112_{FcµR}$ (Extended Data Fig. 6g).

Similar to the situation in the FcµR–Fcµ–J complex, a maximum of four FcµR molecules was observed to attach to Fcµ–J–SC. No FcµR is bound to Fcµ1A, even though the binding site appears exposed at first glance. Superimposing an FcµR-D1–Fcµ-Cµ4 pair from the crystal structure to Fcµ1A suggests that the binding of this fifth FcµR would lead to unfavourable packing with the R4' FcµR (Fig. 3c). Fcµ1A is bound to the C-terminal hairpin of the J-chain, and this interaction apparently leads to a slight tilting of Fcµ1 within the Fcµ–J plane. Therefore, FcµR would have to approach the Fcµ–J platform with a slightly different angle at this site when compared with R2'–R4', leading to a clash with the R4' FcµR.
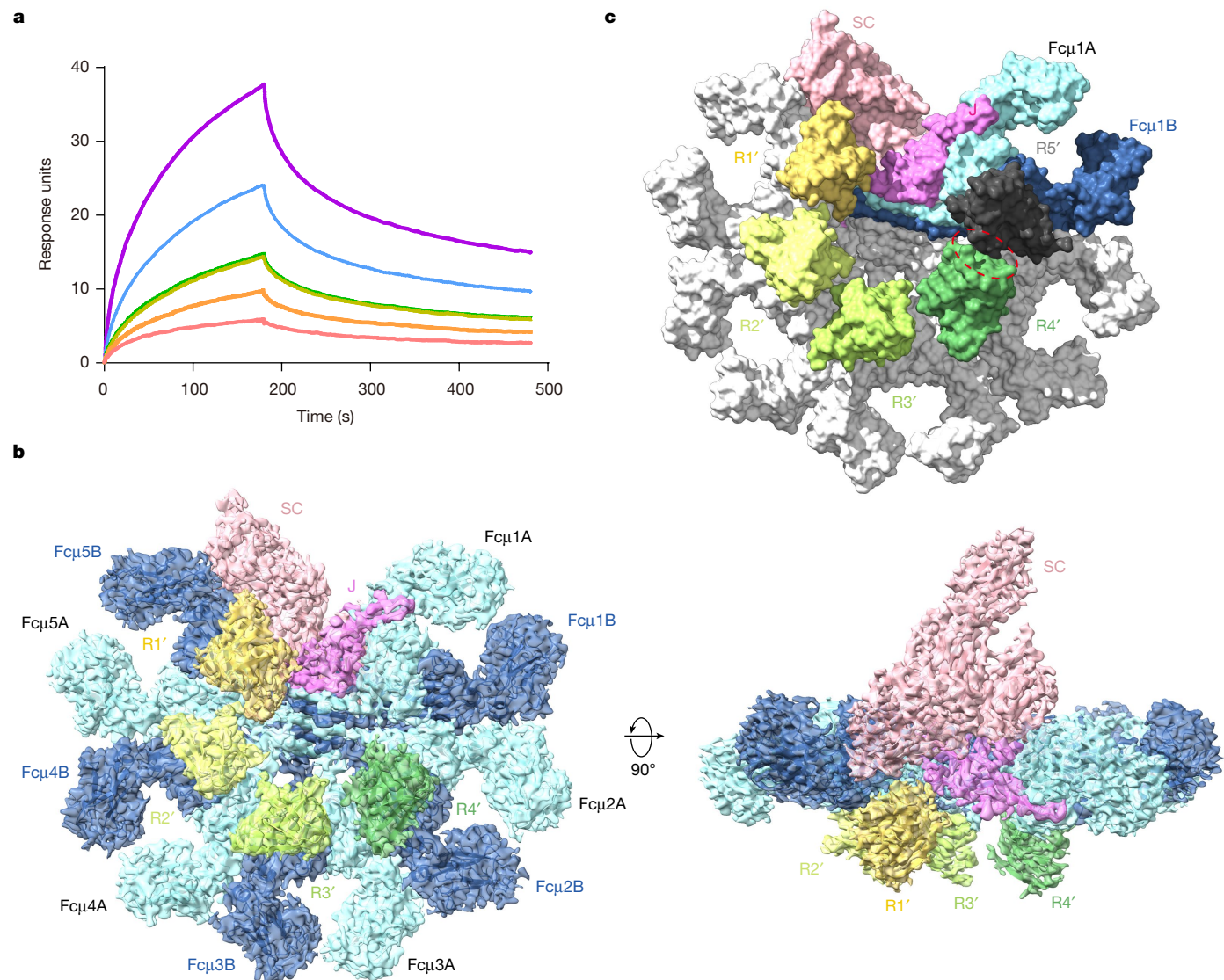
Fig. 3 | Cryo-EM structure of the FcμR-ECD–Fcμ–J–SC complex. a, SPR analyses of the interactions between FcμR-D1 and Fcμ–J–SC performed by passing twofold serial dilutions of Fcμ–J–SC (from 40 nM to 2.5 nM) to immobilized FcμR-D1. Fcμ–J–SC binding to FcμR-D1 K_d = 2.85 ± 0.16 nM. **b**, Overall structure of the 4:1 FcμR-ECD–Fcμ–J–SC complex shown in two views. The four FcμR molecules are shown in yellow and green and labelled R1′–R4′. SC is shown in pink. **c**, An FcμR molecule bound to the R5′ site (black) would lead to unfavourable packing with the R4′ FcμR (green), as indicated by the dashed circle.

FcμR mutants with reduced binding to IgM

To assess the functional relevance of the molecular interactions described above, we designed FcμR mutants and performed functional experiments. The R45A mutant of FcμR-D1 failed to pull down monomeric Fcμ (Fig. 4a). Likewise, R45A, F67A;K69A, N109A;R112A, R45A;F67A, R45A;R112A and R45A;F67A;R112A all displayed reduced or abolished interactions with Fcμ–J (Fig. 4b) and Fcμ–J–SC (Fig. 4c). To examine the FcμR–IgM interaction in a cellular context, we fused wild-type (WT) FcμR or the R45A;F67A mutant to GFP and expressed them in HeLa cells. As shown in Fig. 4d, cells bearing WT FcμR read-ily absorbed Fcμ–J on the surface and quickly internalized it at 37 °C, consistent with previous observations[14,32]. By contrast, IgM binding and internalization were not observed in the R45A;F67A-expressing cells. We also generated HEK293T and Jurkat cell lines stably expressing WT or the R45A;F67A FcμR. Although their cell-surface levels were similar, R45A;F67A-expressing cells captured substantially less Fcμ–J, as evalu-ated by flow cytometry (Fig. 4e and Extended Data Fig. 7). Together, these data corroborate our structural analyses and demonstrate the critical roles of these FcμR residues in binding to IgM.

Discussion

Our results show how FcμR binds mIgM, pIgM and sIgM. We first showed that FcμR can form a 2:1 complex with mIgM. FcμR physically associates with IgM BCR[3] and limits its cell-surface delivery by causing reten-tion in the Golgi apparatus[4]. A universal phenotype manifested by the *Fcmr*-knockout mice is autoantibody production, demonstrating the critical function of FcμR in balancing BCR signalling. In light of the recently reported IgM BCR structure, we showed that the FcμR-binding sites are accessible in IgM BCR. Future work is needed to determine how FcμR, particularly the stalk region and transmembrane segment of FcμR, interacts with Igα and Igβ to regulate BCR activity.

We further showed that FcμR can form a 4:1 complex with both Fcμ–J and Fcμ–J–SC, albeit binding on opposite faces of the Fcμ–J platform. Among the eight different binding sites, the R1 site appears to have the highest affinity, as this site is always occupied in the FcμR–Fcμ–J samples. Furthermore, FcμR-D1 binds with higher affinity to Fcμ–J than to Cμ4, which also reflects the stronger binding at the R1 site, as interac-tions at the R2–R4 sites largely resemble those seen in the FcμR-D1–Cμ4 structure, whereas FcμR interacts with three Fcμ–J subunits at the R1
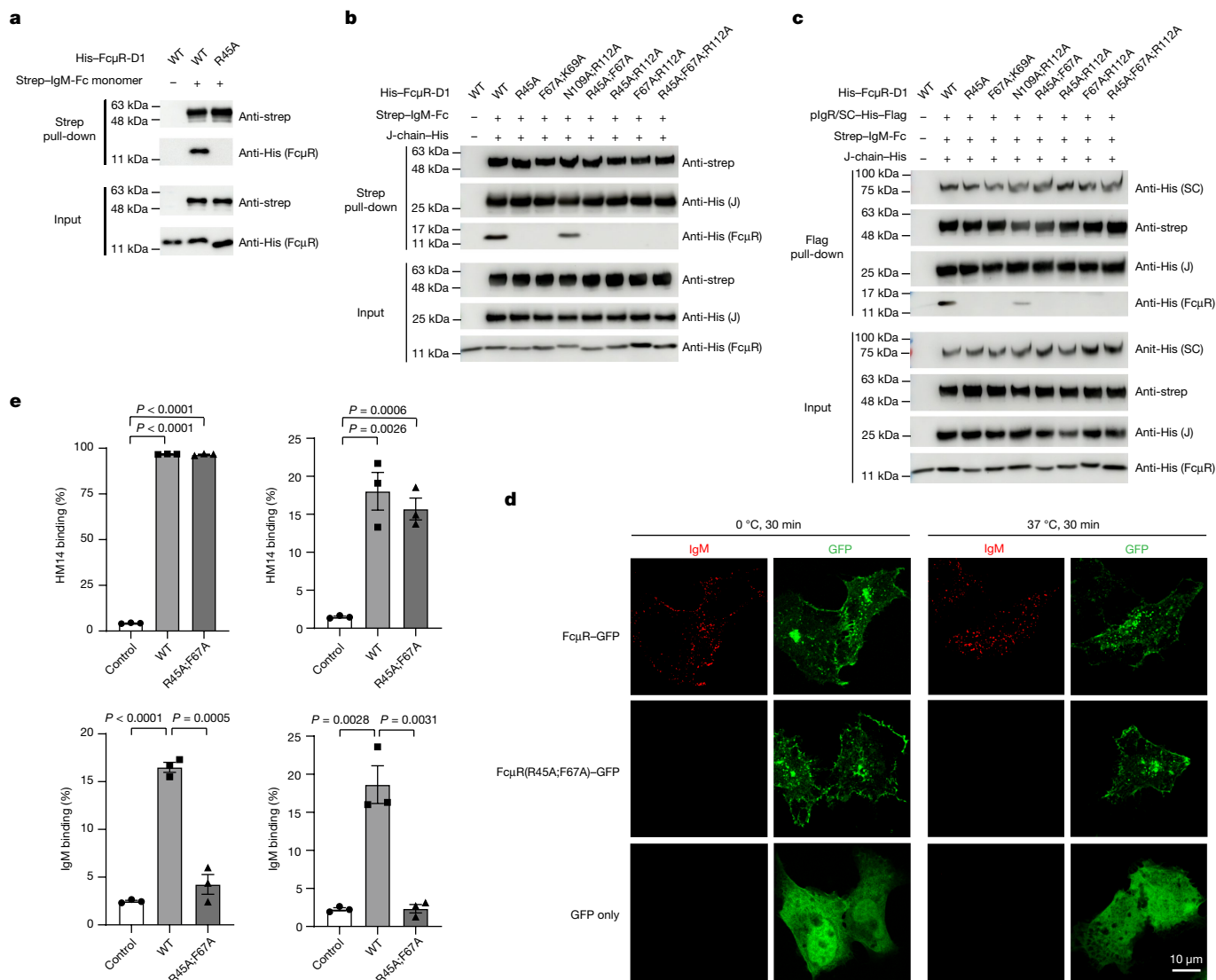
Fig. 4 | FcµR mutants display reduced binding to IgM. a, The FcµR-D1 R45A mutant did not interact with monomeric Fcµ in a pull-down assay. For gel source data in this paper, see Supplementary Fig. 1. All pull-down experiments in this paper were repeated two times. **b**, FcµR-D1 mutants displayed reduced or abolished interaction with Fcµ–J. **c**, FcµR-D1 mutants were also defective in binding to Fcµ–J–SC. **d**, HeLa cells expressing FcµR(R45A;F67A) did not bind and internalize twin-strep-tagged Fcµ–J, as examined by confocal fluorescence microscopy. A twin-strep tag is present on the N terminus of Fcµ, and binding of Fcµ–J was examined using PE-labelled streptavidin (red). Expression of FcµR was monitored with C-terminally fused GFP (green). These images are representatives of 131 of 171 cells (131 Fcµ–J⁺ cells out of 171 GFP⁺ cells) examined

for FcµR–GFP at 0 °C; 22 of 27 cells for FcµR–GFP at 37 °C; 0 of 48 cells for FcµR(R45A;F67A)–GFP at 0 °C; 0 of 16 cells for FcµR(R45A;F67A)–GFP at 37 °C; 0 of 33 cells for GFP only at 0 °C; and 0 of 19 cells for GFP only at 37 °C; respectively. This experiment was repeated two times with similar results. **e**, Flow cytometry analyses suggested that HEK293T (left) and Jurkat (right) cells stably expressing FcµR(R45A;F67A) exhibit reduced binding to Fcµ–J. Cell-surface FcµR levels were examined using the HM14 anti-FcµR antibody. The experiment was repeated three times. The black dots indicate individual data points for $n = 3$ biological replicates. Data were plotted as the mean ± 1 s.e.m. Statistical analysis was performed by two-tailed, unpaired Student's *t*-test, and the *P* values are indicated in the graphs. For data underlying this graph, see the source data.

site. The R1′ site appears to be the second preferred site. When the R1 site is occupied by SC, FcµR binds to the other side of Fcµ–J instead of the R2–R4 positions. Compared with the R2–R4 or R2′–R4′ sites, the R1′ site also features additional interactions between FcµR and the J-chain, as well as the Fcµ1A tailpiece.

The formation of receptor clusters is a common means to initiate signalling events. Our results strongly suggest that four FcµR molecules tend to cluster on one side of pIgM. Once an FcµR binds the R1 or R1′ site, it may help to recruit the other three molecules to the same side via the stalk region. We envision that the formation of such an FcµR tetramer would bring their transmembrane segments and cytosolic regions together to trigger effector functions. The binding of a fifth FcµR is not allowed on either side of pIgM: on the R1–R4 side,

it is hindered by the β2–β3 loop of the J-chain, whereas on the R1′–R4′ side, the modest tilting of Fcµ1 caused by the alliance with the J-chain prevents the binding. Therefore, in addition to preventing IgM hexamer formation, the J-chain appears to break another layer of symmetry, permitting pIgM to bind to only four FcµR molecules on either side. It remains to be determined whether an IgM hexamer that lacks the J-chain can recruit six FcµR molecules and whether this would lead to a different signalling outcome.

Whether pIgM would engage eight FcµR molecules simultaneously on both sides and thereby bridge the contact between two FcµR-bearing cells remains unknown. We did not observe particles with FcµR-ECD or FcµR-D1 bound to both sides of Fcµ–J, even though FcµR-ECD and FcµR-D1 were both present in high excess during sample

Article

preparation. Size-exclusion chromatographies were performed after FcμR-ECD or FcμR-D1 was incubated with Fcμ–J, which probably removed FcμR-ECD and FcμR-D1 that bound weakly. Structural analyses suggest that the presence of R1–R4 FcμR renders a conformational change of the Fcμ–J platform and the R1′–R4′ sites are slightly displaced (Extended Data Fig. 8). Therefore, binding of FcμR at the R1–R4 sites probably reduces its binding to the other side.

Compared with human FcμR, mouse FcμR binds IgM less tightly[2,44]. Differences of two residues may contribute to this difference in binding behaviour (Extended Data Fig. 2b). First, mouse FcμR lacks Asn66, which may impact the positioning of Phe67, which is involved in all of the binding sites described above. Second, Arg112 is replaced by a Lys in mice, which probably affects the binding at the R1 or R1′ sites.

In summary, we delineated the complex mechanism of IgM recognition by its specific receptor FcμR. These results are important steps towards further understanding the elusive effector functions of IgM.

Online content

Any methods, additional references, Nature Portfolio reporting summaries, source data, extended data, supplementary information, acknowledgements, peer review information; details of author contributions and competing interests; and statements of data and code availability are available at https://doi.org/10.1038/s41586-023-05835-w.

1. Heyman, B. & Shulman, M. J. in *Encyclopedia of Immunobiology* (ed. Ratcliffe, M. J. H.) 1–14 (Academic Press, 2016).
2. Kubagawa, H. et al. Identity of the elusive IgM Fc receptor (FcμR) in humans. *J. Exp. Med.* **206**, 2779–2793 (2009).
3. Ouchida, R. et al. FcμR interacts and cooperates with the B cell receptor to promote B cell survival. *J. Immunol.* **194**, 3096–3101 (2015).
4. Nguyen, T. T. et al. The IgM receptor FcμR limits tonic BCR signaling by regulating expression of the IgM BCR. *Nat. Immunol.* **18**, 321–333 (2017).
5. Rochereau, N. et al. Essential role of TOSO/FAIM3 in intestinal IgM reverse transcytosis. *Cell Rep.* **37**, 110006 (2021).
6. Li, Y. et al. Structural insights into immunoglobulin M. *Science* **367**, 1014–1017 (2020).
7. Kumar, N., Arthur, C. P., Ciferri, C. & Matsumoto, M. L. Structure of the human secretory immunoglobulin M core. *Structure* **29**, 564–571.e3 (2021).
8. Kumar, N., Arthur, C. P., Ciferri, C. & Matsumoto, M. L. Structure of the secretory immunoglobulin A core. *Science* **367**, 1008–1014 (2020).
9. Wang, Y. et al. Structural insights into secretory immunoglobulin A and its interaction with a pneumococcal adhesin. *Cell Res.* **30**, 602–609 (2020).
10. Kaetzel, C. S. The polymeric immunoglobulin receptor: bridging innate and adaptive immune responses at mucosal surfaces. *Immunol. Rev.* **206**, 83–99 (2005).
11. Akula, S. & Hellman, L. The appearance and diversification of receptors for IgM during vertebrate evolution. *Curr. Top. Microbiol. Immunol.* **408**, 1–23 (2017).
12. Shibuya, A. et al. Fcα/μ receptor mediates endocytosis of IgM-coated microbes. *Nat. Immunol.* **1**, 441–446 (2000).
13. Hitoshi, Y. et al. Toso, a cell surface, specific regulator of Fas-induced apoptosis in T cells. *Immunity* **8**, 461–471 (1998).
14. Shima, H. et al. Identification of TOSO/FAIM3 as an Fc receptor for IgM. *Int. Immunol.* **22**, 149–156 (2010).
15. Honjo, K. et al. Altered Ig levels and antibody responses in mice deficient for the Fc receptor for IgM (FcμR). *Proc. Natl Acad. Sci. USA* **109**, 15882–15887 (2012).
16. Ouchida, R. et al. Critical role of the IgM Fc receptor in IgM homeostasis, B-cell survival, and humoral immune responses. *Proc. Natl Acad. Sci. USA* **109**, E2699–E2706 (2012).
17. Choi, S. C. et al. Mouse IgM Fc receptor, FCMR, promotes B cell development and modulates antigen-driven immune responses. *J. Immunol.* **190**, 987–996 (2013).
18. Liu, J. et al. Fcμ receptor promotes the survival and activation of marginal zone B cells and protects mice against bacterial sepsis. *Front. Immunol.* **9**, 160 (2018).
19. Yu, J. et al. Surface receptor Toso controls B cell-mediated regulation of T cell immunity. *J. Clin. Invest.* **128**, 1820–1836 (2018).
20. Liu, J. et al. Role of the IgM Fc receptor in immunity and tolerance. *Front. Immunol.* **10**, 529 (2019).
21. Kubagawa, H. et al. Functional roles of the IgM Fc receptor in the immune system. *Front. Immunol.* **10**, 945 (2019).
22. Meryk, A. et al. Fcμ receptor as a costimulatory molecule for T cells. *Cell Rep.* **26**, 2681–2691.e5 (2019).
23. Gaublomme, J. T. et al. Single-cell genomics unveils critical regulators of Th17 cell pathogenicity. *Cell* **163**, 1400–1412 (2015).
24. Lang, K. S. et al. Involvement of Toso in activation of monocytes, macrophages, and granulocytes. *Proc. Natl Acad. Sci. USA* **110**, 2593–2598 (2013).
25. Brenner, D. et al. Toso controls encephalitogenic immune responses by dendritic cells and regulatory T cells. *Proc. Natl Acad. Sci. USA* **111**, 1060–1065 (2014).
26. Kubli, S. P. et al. Fcmr regulates mononuclear phagocyte control of anti-tumor immunity. *Nat. Commun.* **10**, 2678 (2019).
27. Skopnik, C. M. et al. Questioning whether IgM Fc receptor (FcμR) is expressed by innate immune cells. *Nat. Commun.* **13**, 3951 (2022).
28. Kubli, S. P., Ramachandran, P., Duncan, G., Brokx, R. & Mak, T. W. Reply to: questioning whether the IgM Fc receptor (FcμR) is expressed by innate immune cells. *Nat. Commun.* **13**, 3950 (2022).
29. Pallasch, C. P. et al. Overexpression of TOSO in CLL is triggered by B-cell receptor signaling and associated with progressive disease. *Blood* **112**, 4213–4219 (2008).
30. Proto-Siqueira, R. et al. SAGE analysis demonstrates increased expression of TOSO contributing to Fas-mediated resistance in CLL. *Blood* **112**, 394–397 (2008).
31. Li, F. J. et al. Enhanced levels of both the membrane-bound and soluble forms of IgM Fc receptor (FcμR) in patients with chronic lymphocytic leukemia. *Blood* **118**, 4902–4909 (2011).
32. Vire, B., David, A. & Wiestner, A. TOSO, the Fcμ receptor, is highly expressed on chronic lymphocytic leukemia B cells, internalizes upon IgM binding, shuttles to the lysosome, and is downregulated in response to TLR activation. *J. Immunol.* **187**, 4040–4050 (2011).
33. Vire, B. et al. Harnessing the Fcμ receptor for potent and selective cytotoxic therapy of chronic lymphocytic leukemia. *Cancer Res.* **74**, 7510–7520 (2014).
34. Faitschuk, E., Hombach, A. A., Frenzel, L. P., Wendtner, C. M. & Abken, H. Chimeric antigen receptor T cells targeting Fcμ receptor selectively eliminate CLL cells while sparing healthy B cells. *Blood* **128**, 1711–1722 (2016).
35. Kubagawa, H. et al. Authentic IgM Fc receptor (FcμR). *Curr. Top. Microbiol. Immunol.* **408**, 25–45 (2017).
36. Nyamboya, R. A., Sutton, B. J. & Calvert, R. A. Mapping of the binding site for FcμR in human IgM-Fc. *Biochim. Biophys. Acta Proteins Proteom.* **1868**, 140266 (2020).
37. Caaveiro, J. M., Kiyoshi, M. & Tsumoto, K. Structural analysis of Fc/FcγR complexes: a blueprint for antibody design. *Immunol. Rev.* **268**, 201–221 (2015).
38. Sutton, B. J. & Davies, A. M. Structure and dynamics of IgE–receptor interactions: FcεRI and CD23/FcεRII. *Immunol. Rev.* **268**, 222–235 (2015).
39. Herr, A. B., Ballister, E. R. & Bjorkman, P. J. Insights into IgA-mediated immune responses from the crystal structures of human FcαRI and its complex with IgA1-Fc. *Nature* **423**, 614–620 (2003).
40. Su, Q. et al. Cryo-EM structure of the human IgM B cell receptor. *Science* **377**, 875–880 (2022).
41. Ma, X. et al. Cryo-EM structures of two human B cell receptor isotypes. *Science* **377**, 880–885 (2022).
42. Dong, Y. et al. Structural principles of B-cell antigen receptor assembly. *Nature* **612**, 156–161 (2022).
43. Ji, C. et al. *Plasmodium falciparum* has evolved multiple mechanisms to hijack human immunoglobulin M. Preprint at *bioRxiv* https://doi.org/10.1101/2022.08.03.502706 (2022).
44. Kubagawa, H. et al. Differences between human and mouse IgM Fc receptor (FcμR). *Int. J. Mol. Sci.* **22**, 7024 (2021).

Methods

Cell culture

Sf21, High Five, HEK293F, HEK293T and HeLa cells were originally purchased from the American Type Culture Collection. Human Jurkat T cells, originally purchased from the American Type Culture Collection, were kindly provided by J. Hu (Peking University). These cell lines were not otherwise authenticated. The cells were regularly tested for free of mycoplasma contamination by standard PCR method. Sf21 and High Five cells were maintained using a nonhumidified shaker at 27 °C in SIM-SF and SIM-HF media (Sino Biological), respectively. HEK293F cells were cultured in a humidified shaker with 5% CO_2 and 55% humidity at 37 °C in SMM 293T-I (Sino Biological). HeLa and HEK293T cells were cultured in DMEM (Gibco) supplemented with 1% penicillin–streptomycin (Gibco) and 10% FBS (Gibco) in a humidified incubator at 37 °C with 5% CO_2. Human Jurkat T cells were cultured in RPMI-1640 medium supplemented with 2 mM GlutaMAX (Gibco), 15% FBS, 10 mM HEPES (Gibco), 1 mM sodium pyruvate (Gibco), 1% MEM nonessential amino acid solution (Gibco) and 1% penicillin–streptomycin at 37 °C and 5% CO_2.

Protein expression and purification

DNA fragments encoding the FcμR-D1 domain (residues 18–124, UniProtKB: O60667) or FcμR-ECD (residues 18–251) were cloned into the pFastBac vector with an N-terminal melittin signal peptide followed by a His_{10} tag. Bacmids were generated using the Bac-to-Bac system (Invitrogen). Recombinant baculoviruses were generated and amplified using Sf21 insect cells. For protein production, High Five cells were infected at a density of 1.5–2.0 million cells per millilitre. After 48 h, the conditioned medium was collected by centrifugation and dialysed to exchange into the binding buffer (25 mM Tris-HCl, pH 8.0, and 150 mM NaCl). The recombinant proteins were then isolated using Ni-NTA affinity purification and eluted with the binding buffer supplemented with 500 mM imidazole. The FcμR-D1 domain and FcμR-ECD were further purified using a Superdex 75 column (GE Healthcare) and a Superdex 200 Increase column (GE Healthcare), respectively. The final buffer used for the gel filtration was the same as the binding buffer. FcμR-D1 mutants were expressed and purified similarly to WT FcμR-D1. The DNA fragment encoding Fcμ residues 446–558 was cloned into a modified pcDNA vector with an N-terminal IL-2 signal peptide and a C-terminal His_8 tag. The plasmid was transiently transfected into HEK293F cells using polyethylenimine (PEI; Polysciences). Four days after transfection, the Fcμ-Cμ4 domain was purified from the conditioned medium by a similar method to FcμR-D1. The Fcμ-J complex was expressed and purified as previously described[6]. For the pull-down assay, Fcμ constructs with an N-terminal twin-strep tag were transiently transfected into HEK293F cells and cultured for 4 days. The protein was retrieved from the conditioned medium using the Strep-Tactin resin (Smart Lifesciences) and then further purified using a Superdex 200 Increase column in buffer containing 25 mM Tris-HCl, pH 7.4, and 150 mM NaCl.

SPR

SPR experiments were performed using a Biacore T200 (GE Healthcare). Purified FcμR-D1 was diluted to 0.02 mg ml^{-1} with 10 mM sodium acetate (pH 5.0), and immobilized on a CM5 chip (Cytiva) to 800–1,100 resonance units (RU) using standard amine coupling chemistry according to the manufacturer instructions. Binding studies were performed by passing twofold serial dilutions of purified Cμ4 (from 80 nM to 5 nM), Fcμ-J (from 2 nM to 0.125 nM), anti-CD20 IgM (from 2 nM to 0.125 nM) or Fcμ-J-SC (from 40 nM to 2.5 nM) over the immobilized FcμR-D1. The running buffer contains 10 mM HEPES, pH 7.4, 150 mM NaCl, 3 mM EDTA and 0.05% (v/v) surfactant P20. The SPR results were analysed with Biacore Evaluation Software and fitted using a 1:1 binding model. Each SPR experiment was repeated at least two times.

Crystallization and structure determination

Purified Fcμ-Cμ4 was incubated with excess FcμR-D1 overnight on ice, and the FcμR-D1–Fcμ-Cμ4 complex was then isolated using a Superdex 75 column and eluted in the final buffer. The purified complex was concentrated to 6–7 mg ml^{-1} for crystallization. Diffraction-quality crystals were grown at 18 °C by the sitting-drop vapour diffusion method using a 1:1 ratio of protein:reservoir solution. The reservoir solution contains 0.1 M ammonium citrate tribasic (pH 7.0) and 12% (w/v) PEG 3,350. For data collection, crystals were transferred into a solution containing 0.1 M ammonium citrate tribasic (pH 7.0), 14% (w/v) PEG 3,350 and 24% ethylene glycol before being cryo-preserved in liquid nitrogen. The diffraction data were collected at the National Facility for Protein Science Shanghai (beamline BL19U). Data were processed using HKL2000 (HKL Research). The crystal structure was determined by molecular replacement using the program Phaser[45]. The Fcμ-Cμ4 domain in the published structure of Fcμ-J-SC (PDB ID: 6KXS) and the model of the FcμR-D1 domain generated by Swiss-Model[46] were used as search models. The structure model was then manually adjusted in Coot[47] and refined using Phenix[48]. The final structure was validated with the wwPDB server[49].

Cryo-EM sample preparation and data collection

To obtain the FcμR-ECD–Fcμ-J complex for cryo-EM analysis, purified Fcμ-J and FcμR-ECD were mixed in a 1:10 molar ratio and incubated on ice for 2 h. After that, the complex was further purified using a Superose 6 Increase column and eluted with the final buffer. The FcμR-ECD–Fcμ-J-SC complex was obtained similarly. For the FcμR-D1–Fcμ-J complexes, purified Fcμ-J and FcμR-D1 were mixed in 1:10 or 1:200 molar ratios and incubated on ice for 2 h. Each sample was also passed through the Superose 6 increase column and eluted using the final buffer. The above samples were then concentrated to 0.6 mg ml^{-1} and crosslinked with 0.05% glutaraldehyde (Sigma-Aldrich) for 10 min at 20 °C. Cryo-grids were prepared using the Vitrobot Mark IV (FEI). A 4 μl protein sample was applied onto holey-carbon gold grids (R1.2/1.3, Quantifoil) or graphene oxide-coated holey-carbon gold grids (R1.2/1.3, EMR), blotted with filter papers (Whatman No. 1) at 4 °C and 100% humidity, and then plunged into liquid ethane. The grids were first screened using a 200 kV Talos Arctica microscope equipped with a Ceta camera (FEI). Data collection was carried out using a Titan Krios electron microscope (FEI) operated at 300 kV for the FcμR-ECD–Fcμ-J and FcμR-ECD–Fcμ-J-SC complexes, or the 200 kV Talos Arctica microscope for the FcμR-D1–Fcμ-J complexes. Movies were recorded on a K2 or a K3 summit direct electron detector. Serial EM[50] and EPU (E Pluribus Unum, Thermo Scientific) were used to collect the cryo-EM data.

Cryo-EM data processing and model building

Movie frames were motion-corrected and dose-weighted using the MotionCor2 program[51]. Contrast transfer function correction was performed using Gctf[52]. The rest of the image processing was performed in RELION[53] or cryoSPARC[54]. High-quality micrographs were selected manually, and particles were autopicked by template picking. Particles were initially subjected to several rounds of 2D classification to exclude inaccurate particles and then further subjected to 3D classifications to choose the correct conformation. The favourite classes were selected for 3D refinement to generate the final 3D reconstruction. The local resolution map was analysed using ResMap[55] and displayed using UCSF ChimeraX[56]. The cryo-EM structure of Fcμ-J or Fcμ-J-SC (PDB ID: 6KXS) and the FcμR-D1 crystal structure were docked into the cryo-EM density map using UCSF Chimera. The structure models were then adjusted using Coot and refined using the real-space refinement in Phenix[57].

Immunoprecipitation

Codon-optimized DNAs encoding the heavy chain (variable domain of VRC01[58] and constant domain of μ-chain) and light chain (variable

Article

domain of VRC01 and constant domain of κ-chain) of mIgM were cloned into the pcDNA vector, separated by a P2A-peptide motif. A Flag tag was present at the N terminus of the light chain. The Igα/Igβ expression vector was constructed similarly, with each of them carrying a C-terminal twin-strep tag. A truncated form of FcμR (residues 1–358; to remove the internalization motif) with a haemagglutinin (HA) tag was also cloned into the pcDNA vector. These plasmids were co-transfected into HEK293T cells using PEI. Cells were harvested 18–24 h later, washed with PBS and resuspended in the lysis buffer containing 25 mM Tris-HCl, pH 8.0, 150 mM NaCl, 1 mM phenylmethylsulfonyl fluoride (PMSF) and 1× protease inhibitor cocktail (B14002, Biotool). The resuspended cell pellets were then solubilized in the lysis buffer supplied with 1% *n*-dodecyl-β-D-maltoside (DDM; Anatrace) and 0.1% cholesteryl hemisuccinate (CHS; Anatrace) at 4 °C for 2 h with mild rotation. After centrifugation, the supernatants were incubated with the anti-Flag M2 affinity gel (A2220, Sigma-Aldrich) for 2 h with mild rotation. The beads were then washed three times using the binding buffer containing 25 mM Tris-HCl, pH 8.0, 150 mM NaCl, 0.1% DDM and 0.01% CHS. The immunoprecipitated proteins were eluted using the binding buffer supplemented with 200 μg ml^{-1} 3× Flag peptide (NJP50002, NJPeptide). The results were analysed by immunoblotting using antibodies to the strep tag (1:3,000; HX1816, HuaxingBio), Flag tag (1:1,000; F3165, Sigma-Aldrich), HA tag (1:1,000; H3663, Sigma-Aldrich) and goat anti-mouse IgG horseradish peroxidase (1:5,000; HS201-01, TransGen Biotech).

Pull-down assay

A twin-strep tag is present on the N terminus of Fcμ. To examine the interaction between the Fcμ monomer or Fcμ–J and FcμR-D1, 40 μg of monomeric Fcμ or Fcμ–J was mixed with purified WT FcμR-D1 or mutants and incubated on ice for 1 h. The mixtures were then incubated with Strep-Tactin resins (Smart Lifesciences) in binding buffer supplemented with 0.1% Triton X-100 at 4 °C for another hour. After incubating at 4 °C for another hour with mild rotation, the Strep-Tactin beads were spun down and washed three times using the binding buffer. Proteins retained on the beads were then eluted using the binding buffer supplemented with 10 mM desthiobiotin (IBA Lifesciences). To examine the interaction between Fcμ–J–SC and FcμR-D1, the Flag tag on the N terminus of SC was used to perform a pull-down experiment with Flag agarose (Sigma-Aldrich). The experimental process was similar to that in the strep pull-down assay described above, except that the binding proteins were eluted using 200 μg ml^{-1} Flag peptide. The results were analysed by immunoblotting using antibodies to the strep tag (1:3,000; HX1816, HuaxingBio) and His tag (1:3,000; HT501, TransGen Biotech).

Confocal fluorescence microscopy

HeLa cells grown on coverslips were transfected with the indicated constructs using PEI and cultured for 24 h. The twin-strep-tagged Fcμ–J complex was first incubated with P-phycoerythrin (PE)-labelled streptavidin (1:333; 12-4317-87, Invitrogen) on ice for 30 min and then added to the cell culture to a final concentration of 15 μg ml^{-1}. After incubation on ice or at 37 °C for an additional 30 min, the cells were washed twice using ice-cold or 37 °C PBS as indicated and fixed with 4% paraformaldehyde. The final coverslips were washed twice and mounted on slides with the fluorescence mounting medium (Dako). Images were acquired using a Nikon Live SR CSU W1 confocal microscope equipped with the ×100/1.4 objective. Images were processed using Fiji (ImageJ) with brightness and contrast adjustment for the whole image.

Preparation of FcμR stable cell lines and flow cytometry

GFP only, FcμR–GFP and the R45A;F67A–GFP mutant were cloned into the pQXCIP vector. These constructs were transfected into the HEK293T cell line together with the helper plasmid pCL10A1 using X-tremeGENE 9 (Roche). Two days later, the culture supernatants containing viruses

were collected, filtered and used to infect Jurkat cells. Fresh medium with 4 μg ml^{-1} puromycin was added to the remaining HEK293T culture to screen for stable HEK293T cell lines overexpressing FcμR and the mutant. For the Jurkat T cell line, polybrene (Sigma-Aldrich) was added to a final concentration of 10 μg ml^{-1} before infecting cells at a ratio of 1×10^6 cells per millilitre of the supernatant. Transfection was performed by centrifugation at 500g for 90 min. Jurkat cells expressing comparable levels of GFP were maintained in the medium containing puromycin at 1 μg ml^{-1} and enriched three times from each transductant using a BD FACSAria III cell sorter (BD Biosciences). Flow cytometric analyses of cell-surface levels of FcμR were performed using the PE-labelled anti-FcμR monoclonal antibody (1:20; 563018, BD Biosciences). To examine IgM binding, cells were incubated with the twin-strep-tagged Fcμ–J complex at a concentration of 15 μg ml^{-1} for 30 min on ice, washed and then incubated with PE-labelled streptavidin. Stained cells were measured by the CytoFLEX S system (Beckman Coulter), and the flow cytometric data were analysed with FlowJo software (Tree Star) and GraphPad Prism.

Reporting summary

Further information on research design is available in the Nature Portfolio Reporting Summary linked to this article.

Data availability

Cryo-EM density maps of FcμR–Fcμ–J and FcμR–Fcμ–J–SC have been deposited in the Electron Microscopy Data Bank with accession codes EMD-34085 (1:1), EMD-34086 (4:1) and EMD-34074. Structural coordinates have been deposited in the PDB with the accession codes 7YTC, 7YTD and 7YSG. The crystal structure of FcμR-D1–Fcμ-Cμ4 has been deposited in the PDB with the accession code 7YTE. The cryo-EM structure of Fcμ–J–SC was determined previously and is available from the PDB under the accession code 6KXS. Source data are provided with this paper.

45. McCoy, A. et al. Phaser (CCP4: supported program) NAME phaser-2.5. 0-maximum likelihood analysis and phasing. SYNOPSIS phaser. *J. Appl. Cryst.* **40**, 658–674 (2007).
46. Biasini, M. et al. SWISS-MODEL: modelling protein tertiary and quaternary structure using evolutionary information. *Nucleic Acids Res.* **42**, W252–W258 (2014).
47. Emsley, P., Lohkamp, B., Scott, W. G. & Cowtan, K. Features and development of Coot. *Acta Crystallogr. D Biol. Crystallogr.* **66**, 486–501 (2010).
48. Adams, P. D. et al. PHENIX: a comprehensive Python-based system for macromolecular structure solution. *Acta Crystallogr. D Biol. Crystallogr.* **66**, 213–221 (2010).
49. Berman, H., Henrick, K. & Nakamura, H. Announcing the worldwide Protein Data Bank. *Nat. Struct. Mol. Biol.* **10**, 980 (2003).
50. Mastronarde, D. N. Automated electron microscope tomography using robust prediction of specimen movements. *J. Struct. Biol.* **152**, 36–51 (2005).
51. Zheng, S. Q. et al. MotionCor2: anisotropic correction of beam-induced motion for improved cryo-electron microscopy. *Nat. Methods* **14**, 331–332 (2017).
52. Zhang, K. Gctf: real-time CTF determination and correction. *J. Struct. Biol.* **193**, 1–12 (2016).
53. Zivanov, J. et al. New tools for automated high-resolution cryo-EM structure determination in RELION-3. *eLife* **7**, e42166 (2018).
54. Punjani, A., Rubinstein, J. L., Fleet, D. J. & Brubaker, M. A. cryoSPARC: algorithms for rapid unsupervised cryo-EM structure determination. *Nat. Methods* **14**, 290–296 (2017).
55. Kucukelbir, A., Sigworth, F. J. & Tagare, H. D. Quantifying the local resolution of cryo-EM density maps. *Nat. Methods* **11**, 63–65 (2014).
56. Pettersen, E. F. et al. UCSF ChimeraX: structure visualization for researchers, educators, and developers. *Protein Sci.* **30**, 70–82 (2021).
57. Liebschner, D. et al. Macromolecular structure determination using X-rays, neutrons and electrons: recent developments in Phenix. *Acta Crystallogr. D Struct. Biol.* **75**, 861–877 (2019).
58. Zhou, T. et al. Structural basis for broad and potent neutralization of HIV-1 by antibody VRC01. *Science* **329**, 811–817 (2010).

Additional information
Supplementary information The online version contains supplementary material available at https://doi.org/10.1038/s41586-023-05835-w.
**Correspondence and requests for materials** should be addressed to Junyu Xiao.
Peer review information *Nature* thanks Falk Nimmerjahn, Beth Stadtmueller and the other, anonymous, reviewer(s) for their contribution to the peer review of this work. Peer reviewer reports are available.
Reprints and permissions information is available at http://www.nature.com/reprints.

Article

a

Cμ4
K_D = 3.80 nM   Chi² = 0.29

Fcμ-J
K_D = 0.22 nM   Chi² = 0.11

Anti-CD20 IgM
K_D = 0.13 nM   Chi² = 2.80

Fcμ-J-SC
K_D = 3.01 nM   Chi² = 0.76

Cμ4
K_D = 2.53 nM   Chi² = 0.30

Fcμ-J
K_D = 0.43 nM   Chi² = 0.46

Anti-CD20 IgM
K_D = 0.38 nM   Chi² = 3.79

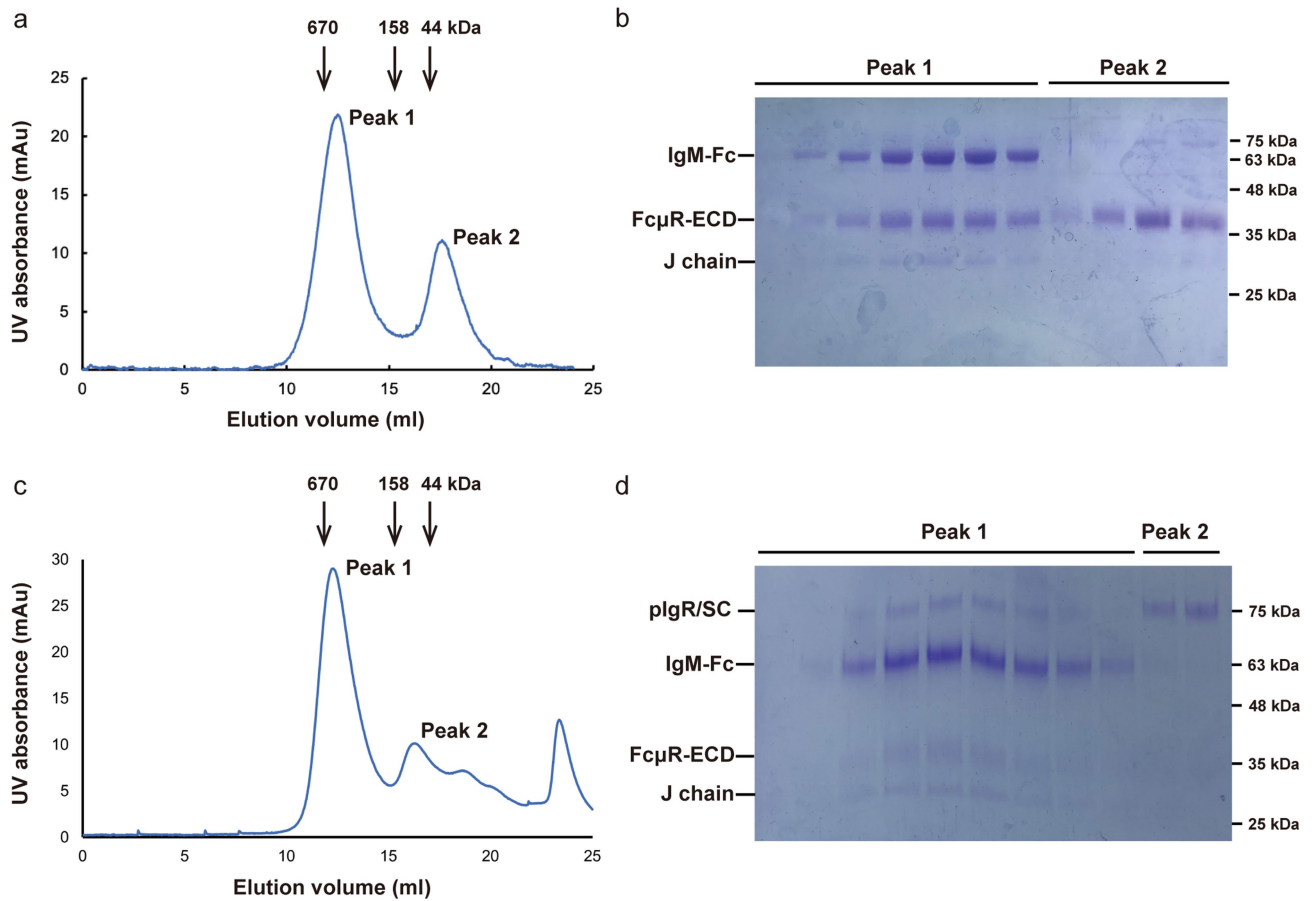**Fcμ-J-SC**
K_D = 2.69 nM   Chi² = 3.21

b

c
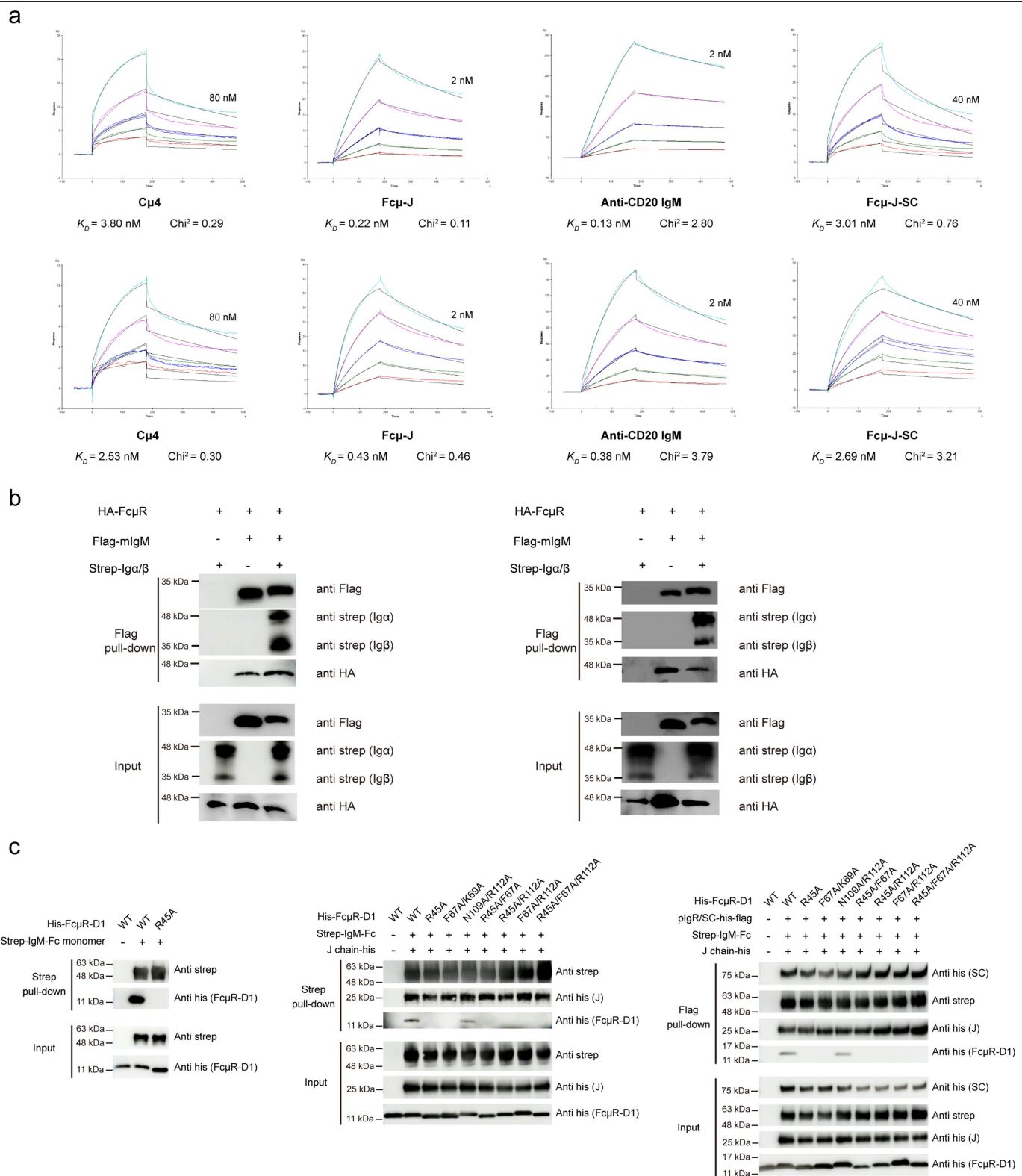
Extended Data Fig. 1 | SPR, coimmunoprecipitation, and pull-down experiments. a. Two repeats of the SPR experiments. The SPR experiments were performed by passing over immobilized FcμR-D1 with two-fold serial dilutions of purified Cμ4, Fcμ–J, anti-CD20 IgM, or Fcμ–J–SC, and the highest concentration values are indicated in the graphs. The original SPR sensorgrams are shown in colored lines, whereas the fitted models are overlaid on the sensorgrams and shown in black. The sensorgrams in the first repeat are shown in the main figures. The model fitting statistics are also shown. **b**. Coimmunoprecipitation of FcμR with mIgM. Results of two independent experiments are shown. **c**. Repeat of the pull-down experiment presented in Fig. 4.
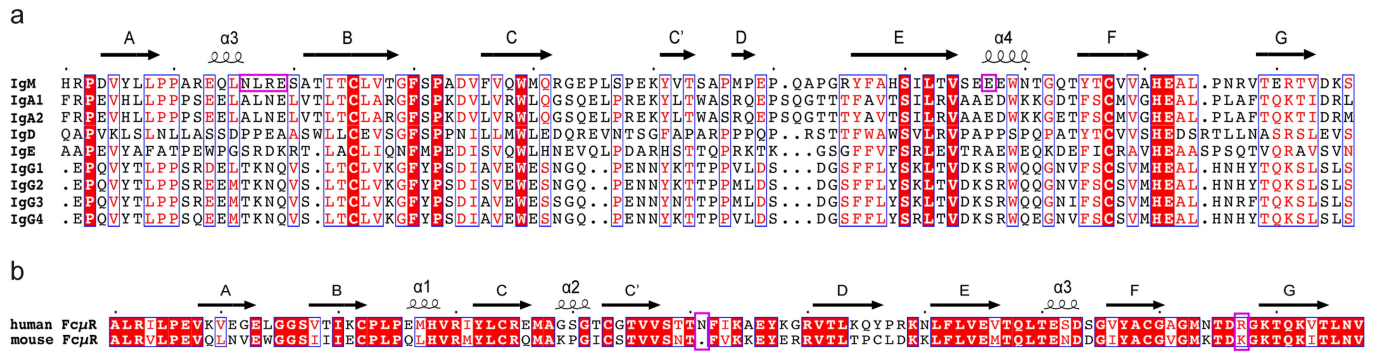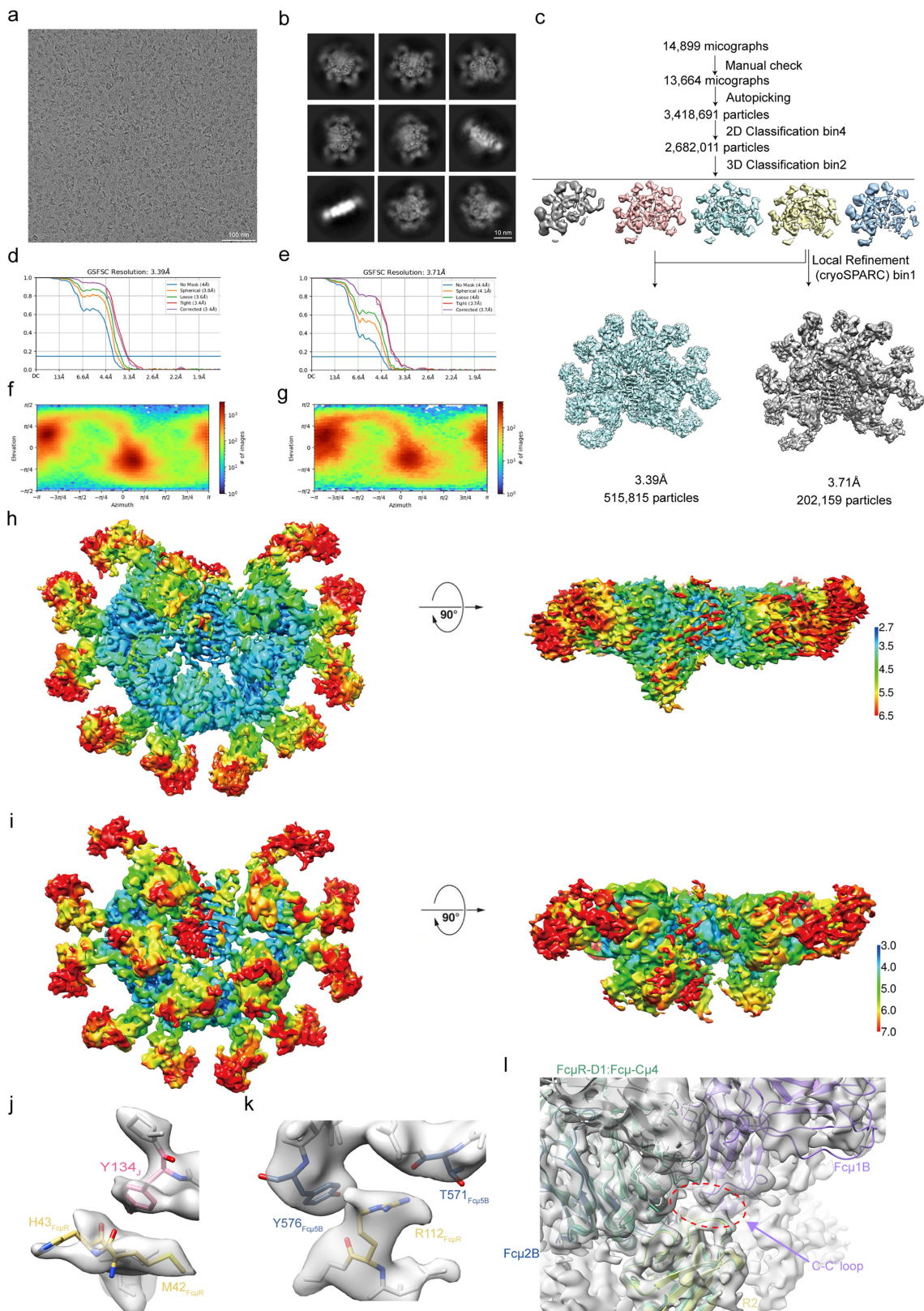
Extended Data Fig. 2 | Sequence alignments of antibody Fc sequences and FcµR. a. Sequence alignment of human antibody Fc sequences. Fcµ residues that are recognized by FcµR are highlighted with magenta rectangles. **b.** Sequence comparison between human FcµR and the mouse protein.

Extended Data Fig. 3 | Purification of the FcµR-ECD–Fcµ–J and FcµR-ECD–Fcµ–J–SC complexes for cryo-EM. a. Size-exclusion chromatography of the FcµR-ECD–Fcµ–J complex on a Superose 6 Increase column. The elution volumes of molecular weight markers are indicated. **b**. SDS–PAGE analyses of the FcµR-ECD–Fcµ–J complex. For gel source data, see Supplementary Fig. 1. All the purification experiments and corresponding SDS-PAGE analyses in this paper have been repeated at least two times with similar results. **c**. Size-exclusion chromatography of the FcµR-ECD–Fcµ–J–SC complex. **d**. SDS–PAGE analyses of the FcµR-ECD–Fcµ–J–SC complex. For gel source data, see Supplementary Fig. 1.

a

b

10 nm

c

14,899 micrographs
↓ Manual check
13,664 micrographs
↓ Autopicking
3,418,691 particles
↓ 2D Classification bin4
2,682,011 particles
↓ 3D Classification bin2

Local Refinement
(cryoSPARC) bin1

3.39Å
515,815 particles

3.71Å
202,159 particles

d GSFSC Resolution: 3.39Å

e GSFSC Resolution: 3.71Å

f

g

h

90°

2.7
3.5
4.5
5.5
6.5

i

90°

3.0
4.0
5.0
6.0
7.0

j

Y134$_J$

H43$_{Fc\mu R}$

M42$_{Fc\mu R}$

k

T571$_{Fc\mu 5B}$

Y576$_{Fc\mu 5B}$

R112$_{Fc\mu R}$

l

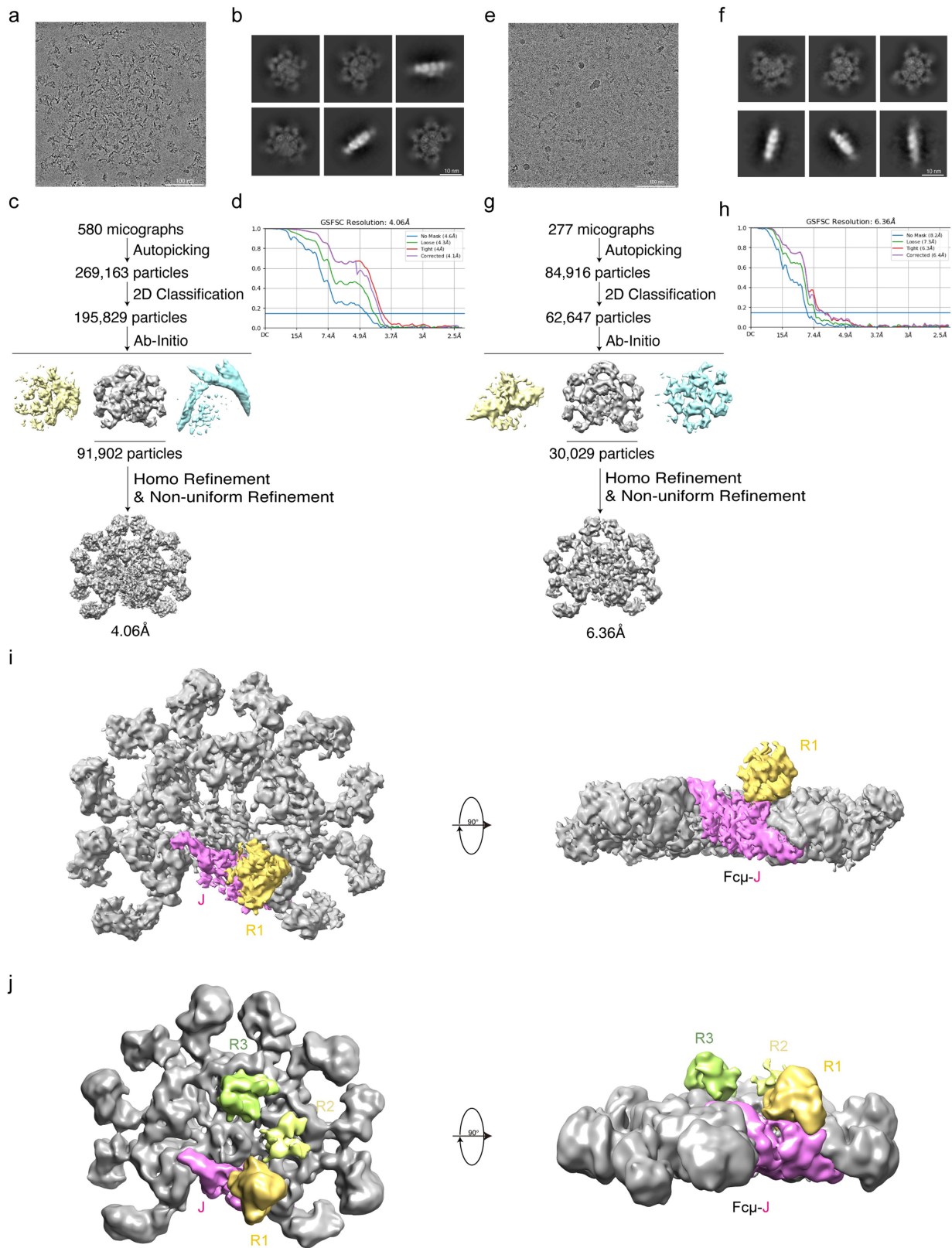FcμR-D1:Fcμ-Cμ4

Fcμ1B

Fcμ2B

C-C' loop

R2
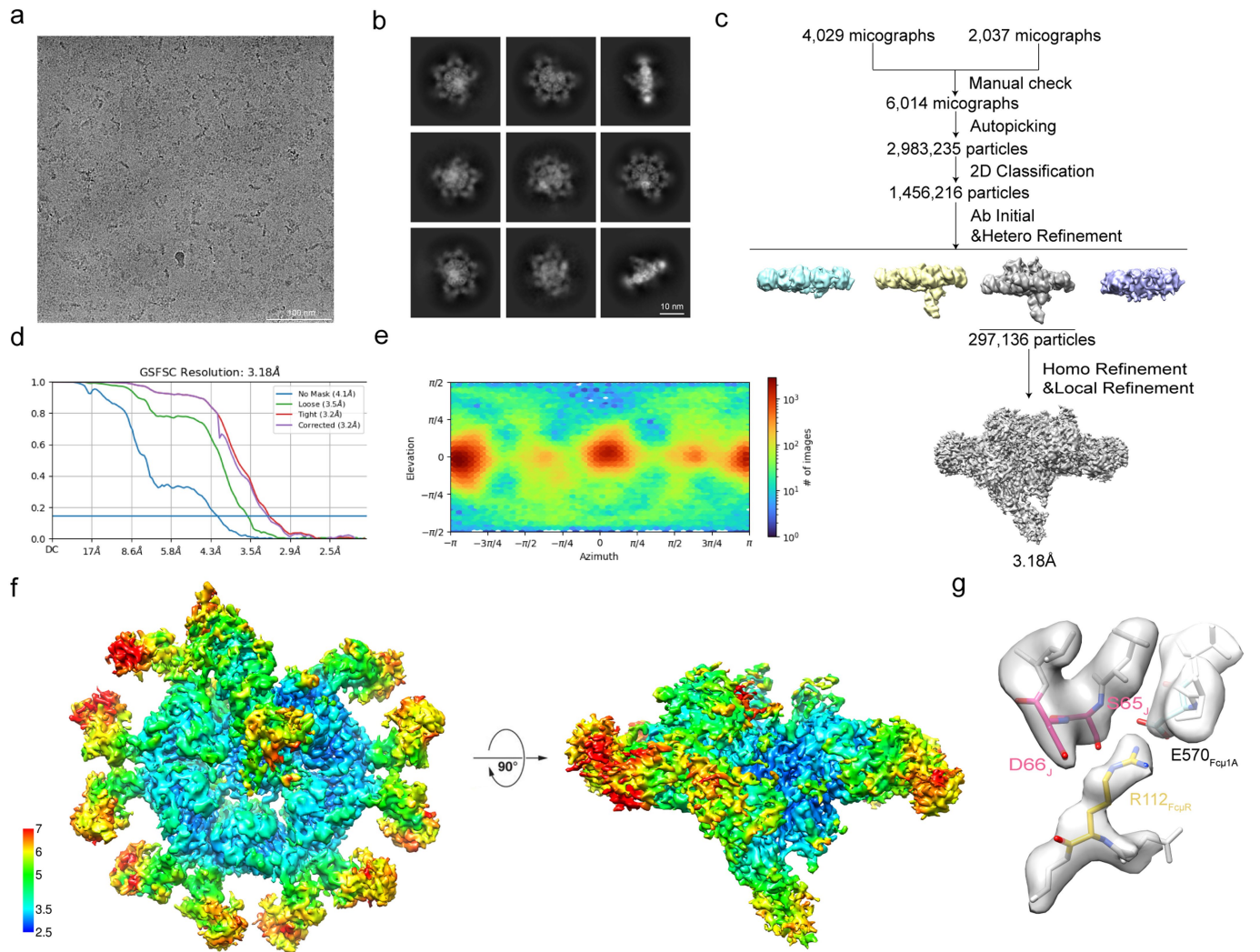
Extended Data Fig. 4 | See next page for caption.

Article

Extended Data Fig. 4 | Cryo-EM 3D reconstruction of the FcμR-ECD–Fcμ–J complex. a. A representative raw cryo-EM image out of 14,899 similar micrographs used for data processing. b. 2D classifications. c. Flow chart for image processing. d. Gold standard Fourier shell correlation (FSC) curves with estimated resolutions of the 1:1 FcμR-ECD–Fcμ–J complex. e. FSC curves of the 4:1 FcμR-ECD–Fcμ–J complex. f. Euler angle distribution of the classified particles for the 1:1 FcμR-ECD–Fcμ–J complex. g. Euler angle distribution of the classified particles for the 4:1 FcμR-ECD–Fcμ–J complex. h. Resolution estimations of the final map of the 1:1 FcμR-ECD–Fcμ–J complex. i. Resolution estimations of the final map of the 4:1 FcμR-ECD–Fcμ–J complex. j. FcμR-D1 interacts with the C-terminal region of the J-chain at the R1 site. k. FcμR-D1 interacts with the tailpiece of Fcμ5B at the R1 site. l. At the R2–R4 sites, in addition to mainly binding to the Cμ4 domains of Fcμ2B, Fcμ3B, and Fcμ4B, FcμR also interacts slightly with the C–C′ loop of Fcμ1B, Fcμ2B, and Fcμ3B from the adjoining Fcμ units. Shown here is a copy of the FcμR-D1–Fcμ-Cμ4 pair from the crystal structure (green) superposed to Fcμ2B, illustrating the close contact between the C–C′ loop of Fcμ1B and the R2 FcμR.

Extended Data Fig. 5 | Cryo-EM analyses of the FcμR-D1–Fcμ–J complex.
a. A representative raw cryo-EM image of the FcμR-D1–Fcμ–J complex
(prepared in a 10:1 molar ratio) out of 580 similar micrographs used for data
processing. **b**. 2D classifications of the sample in **a**. **c**. Flow chart for image
processing of the sample in **a**. **d**. FSC curves with estimated resolutions of the
sample in **a**. **e**. A representative raw cryo-EM image of the FcμR-D1–Fcμ–J complex

(prepared in a 200:1 molar ratio) out of 277 similar micrographs used for data
processing. **f**. 2D classifications of the sample in **e**. **g**. Flow chart for image
processing of the sample in **e**. **h**. FSC curves with estimated resolutions of the
sample in **e**. **i**. 3D reconstruction of the FcμR-D1–Fcμ–J complex prepared in a
10:1 molar ratio. **j**. 3D reconstruction of the FcμR-D1–Fcμ–J complex prepared
in a 200:1 molar ratio.

Article

Extended Data Fig. 6 | Cryo-EM 3D reconstructions of the FcμR-ECD–Fcμ–J–SC complex. a. A representative raw cryo-EM image out of 6,066 similar micrographs used for data processing. **b**. 2D classifications. **c**. Flow chart for image processing. **d**. Gold standard Fourier shell correlation (FSC) curves with estimated resolutions. **e**. Euler angle distribution of the classified particles. **f**. Resolution estimations of the final map. **g**. Arg112$_{FcμR}$ contacts J-chain Ser65$_J$–Asp66$_J$ as well as Glu570 in the tailpiece of Fcμ1A.
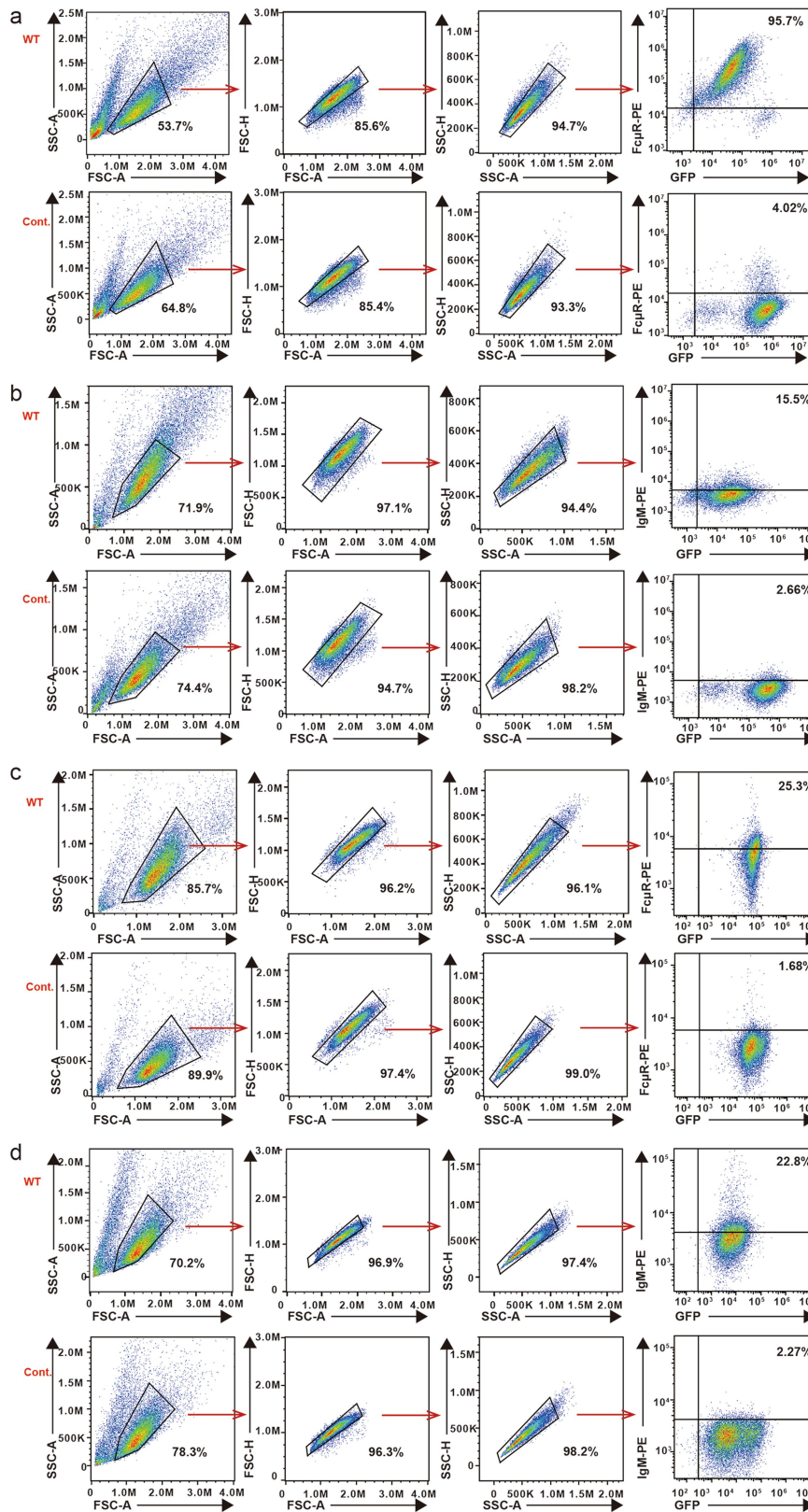
Extended Data Fig. 7 | Gating strategy for the detection of FcµR expression and IgM binding by flow cytometry. a. Gating strategy used to sort HEK293T cells for analyzing the cell surface FcµR levels. The strategy used for the WT FcµR expressing cells is shown, and the R45A/F67A mutant expressing cells were analyzed using the same strategy as WT. Cells stably expressing GFP were used as negative controls (Cont.) to set the level of background. **b.** Gating strategy used to sort HEK293T cells for analyzing IgM binding. **c.** Gating strategy used to sort Jurkat cells for analyzing the cell surface FcµR levels. **d.** Gating strategy used to sort Jurkat cells for analyzing IgM binding.
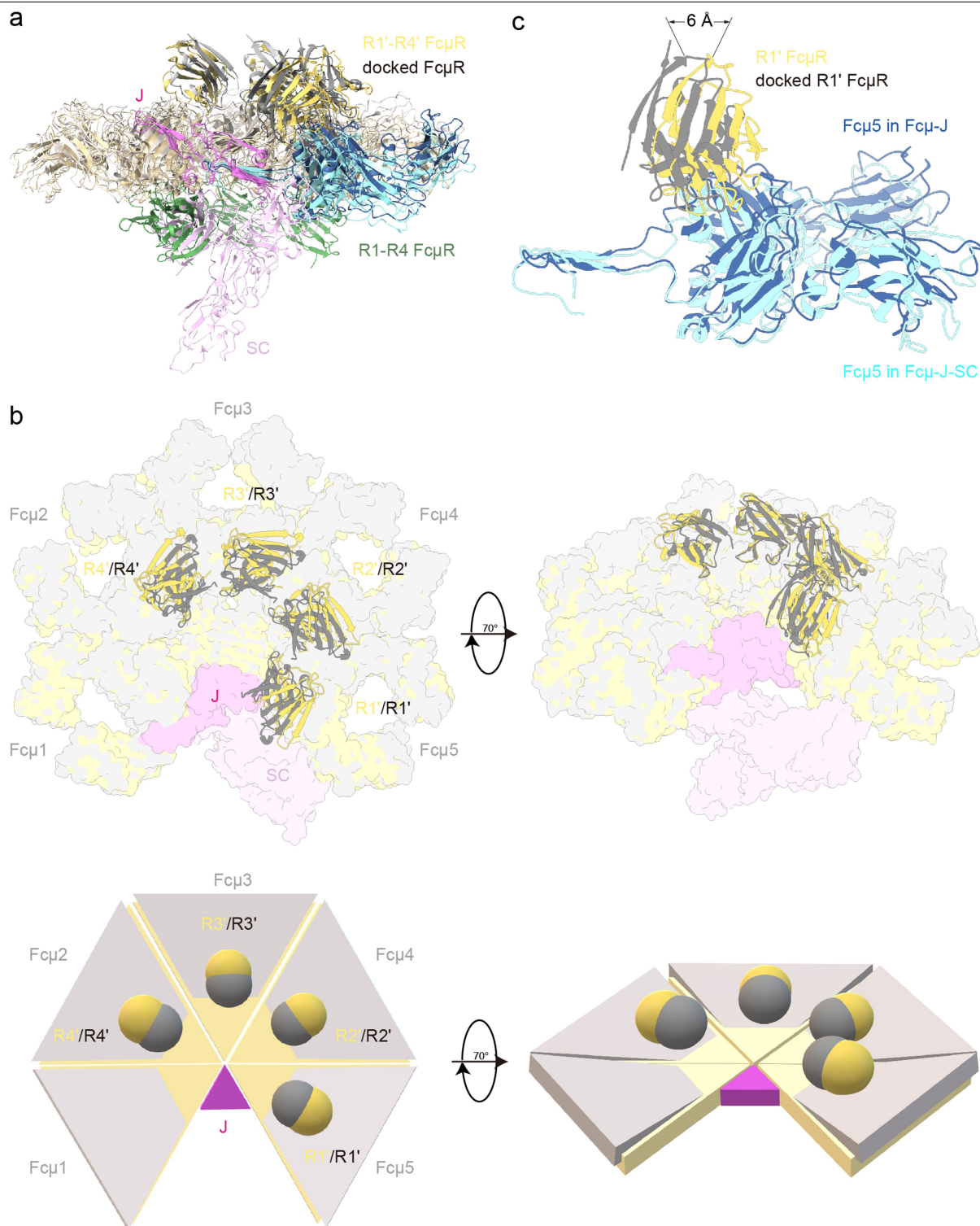
Extended Data Fig. 8 | The binding of FcμR molecules at the R1–R4 sites may reduce the binding of FcμR on the other side. a. FcμR-D1–Fcμ-Cμ4 crystal structures were superposed onto Fcμ2–5 in the 4:1 FcμR–Fcμ-J cryo-EM structure to generate a model with 4 molecules of FcμR bound also at the R1′–R4′ sites (gray). This 8:1 FcμR–Fcμ-J model was then aligned to the FcμR–Fcμ-J–SC cryo-EM structure based on the central tailpiece region and J-chain. The R1–R4 and R1′–R4′ FcμR molecules from the cryo-EM structures are shown in green and yellow, respectively. The Fcμ5 molecules are shown in two shades of blue, whereas the rest Fcμ molecules are shown in light yellow. J-chain and SC are shown in magenta and pink. The presence of FcμR at the R1–R4 side appears to render the Fcμ–J platform slightly concave; and the R1′–R4′ binding sites in the 4:1 FcμR–Fcμ-J structure are slightly displaced compared to the corresponding sites in the FcμR–Fcμ-J–SC complex. **b**. Two different views of the aligned structures in **a** to highlight the structural differences at the R1′–R4′ sites. When compared to the R1′–R4′ FcμR molecules (yellow) in the cryo-EM structure, all four docked FcμR molecules (gray) tilt towards the center of the Fcμ-J platform in the model. A simplified cartoon illustrating these differences is shown below (SC is not depicted in the cartoon). **c**. An enlarged view of the Fcμ5 molecules from the above aligned structures is shown to illustrate the moderate displacement of the R1′ site.

Extended Data Table 1 | Crystal data collection and refinement statistics

	FcμR-D1:Fcμ-Cμ4 (PDB 7YTE)
Data collection	
Space group	P 3
Cell dimensions	
a, b, c (Å)	85.72, 85.72, 60.68
α, β, γ (°)	90, 90, 120
Resolution (Å)	25.47-3.00 (3.11-3.00)
R_{sym} or R_{merge}	0.171 (0.363)
$I / \sigma I$	7.9 (2.6)
Completeness (%)	95.35 (91.79)
Redundancy	2.7 (2.8)
Refinement	
Resolution (Å)	3.00
No. reflections	25,788 (2,435)
R_{work} / R_{free}	0.229 / 0.268
No. atoms	
Protein	3,372
Ligand/ion	0
Water	0
B-factors	
Protein	48.32
Ligand/ion	N/A
Water	N/A
R.m.s. deviations	
Bond lengths (Å)	0.002
Bond angles (°)	0.66

*Each dataset was collected from a single crystal. *Values in parentheses are for highest-resolution shell.

Article

Extended Data Table 2 | Cryo-EM data collection, refinement and validation statistics

	1:1 FcµR:Fcµ-J (EMDB-34085) (PDB 7YTC)	4:1 FcµR:Fcµ-J (EMDB-34086) (PDB 7YTD)	4:1 FcµR:Fcµ-J-SC (EMDB-34074) (PDB 7YSG)
Data collection and processing			
Magnification	165,000	165,000	64,000
Voltage (kV)	300	300	300
Electron exposure (e–/Å^2)	59.74	59.74	50
Defocus range (µm)	-0.8 to -1.6	-0.8 to -1.6	-1.0 to -1.5
Pixel size (Å)	0.828	0.828	1.08
Symmetry imposed	C1	C1	C1
Initial particle images (no.)	3,418,691	3,418,691	2,983,235
Final particle images (no.)	515,815	202,159	297,136
Map resolution (Å) FSC threshold: 0.143	3.39	3.71	3.18
Refinement			
Initial model used (PDB code)	6KXS, 7YTE	6KXS, 7YTE	6KXS, 7YTE
Model resolution (Å) FSC threshold: 0.143	3.39	3.71	3.18
Map sharpening B factor (Å^2)	-143.6	-135.2	-97.8
Model composition			
Non-hydrogen atoms	19,372	21,820	25,695
Protein residues	2,469	2,790	3,288
Ligands	12	12	12
B factors (Å^2)			
Protein	121.93	186.15	108.75
Ligand	85.63	168.02	58.72
R.m.s. deviations			
Bond lengths (Å)	0.003	0.003	0.003
Bond angles (°)	0.714	0.716	0.689
Validation			
MolProbity score	2.06	2.10	2.03
Clashscore	10.85	14.57	15.22
Poor rotamers (%)	0.09	0.04	0.07
Ramachandran plot			
Favored (%)	91.37	93.34	95.08
Allowed (%)	8.63	6.66	4.92
Disallowed (%)	0.00	0.00	0.00

Data were collected using Titan Krios electron microscopes, and recorded using K2 (FcµR–Fcµ–J) and K3 (FcµR–Fcµ–J–SC) direct electron detectors.

nature portfolio

Corresponding author(s): Junyu Xiao

Last updated by author(s): Jan 31, 2023

Reporting Summary

Nature Portfolio wishes to improve the reproducibility of the work that we publish. This form provides structure for consistency and transparency in reporting. For further information on Nature Portfolio policies, see our Editorial Policies and the Editorial Policy Checklist.

Statistics

For all statistical analyses, confirm that the following items are present in the figure legend, table legend, main text, or Methods section.

n/a	Confirmed	
☐	☒	The exact sample size (*n*) for each experimental group/condition, given as a discrete number and unit of measurement
☐	☒	A statement on whether measurements were taken from distinct samples or whether the same sample was measured repeatedly
☐	☒	The statistical test(s) used AND whether they are one- or two-sided *Only common tests should be described solely by name; describe more complex techniques in the Methods section.*
☒	☐	A description of all covariates tested
☒	☐	A description of any assumptions or corrections, such as tests of normality and adjustment for multiple comparisons
☐	☒	A full description of the statistical parameters including central tendency (e.g. means) or other basic estimates (e.g. regression coefficient) AND variation (e.g. standard deviation) or associated estimates of uncertainty (e.g. confidence intervals)
☐	☒	For null hypothesis testing, the test statistic (e.g. *F*, *t*, *r*) with confidence intervals, effect sizes, degrees of freedom and *P* value noted *Give P values as exact values whenever suitable.*
☒	☐	For Bayesian analysis, information on the choice of priors and Markov chain Monte Carlo settings
☒	☐	For hierarchical and complex designs, identification of the appropriate level for tests and full reporting of outcomes
☒	☐	Estimates of effect sizes (e.g. Cohen's *d*, Pearson's *r*), indicating how they were calculated

Our web collection on statistics for biologists contains articles on many of the points above.

Software and code

Policy information about availability of computer code

Data collection	Serial EM (v3.8.7) and EPU (v2.12.1) were used to collect the cryo-EM data.
Data analysis	HKL2000 (v721.4) was used to process the X-ray diffraction data. MotionCor2 (v1.4.4), Gctf (v1.06), cryoSPARC (v3.2) and RELION (v3.1) were used to process the cryo-EM data. The local resolution map was analyzed using ResMap and displayed using UCSF ChimeraX v1.4. Model was docked into map using UCSF Chimera v1.15. Structural modeling and refinement were performed using Coot (v0.9.4.1) and Phenix (v1.19). The flow cytometric data were analyzed with FlowJo software (vx.0.7) and GraphPad Prism (v8.0.2) The SPR data were analyzed with Biacore Evaluation Software (v2.0). Images in confocal fluorescence assay were processed using Fiji (ImageJ) v2.1.0/1.53c.

For manuscripts utilizing custom algorithms or software that are central to the research but not yet described in published literature, software must be made available to editors and reviewers. We strongly encourage code deposition in a community repository (e.g. GitHub). See the Nature Portfolio guidelines for submitting code & software for further information.

Data

Cryo-EM density maps of FcµR:Fcµ-J (1:1 and 4:1) and FcµR:Fcµ-J-SC have been deposited in the Electron Microscopy Data Bank with accession codes EMD-34085, EMD-34086, and EMD-34074. The corresponding structural coordinates have been deposited in the Protein Data Bank (PDB) with accession codes 7YTC, 7YTD, and 7YSG. Crystal structure of FcµR-D1:Fcµ-Cµ4 has been deposited in PDB with accession code 7YTE. The cryo-EM structure of Fcµ-J-SC was determined previously and available from PDB under 6KXS.

Human research participants

Reporting on sex and gender	N/A
Population characteristics	N/A
Recruitment	N/A
Ethics oversight	N/A

Note that full information on the approval of the study protocol must also be provided in the manuscript.

Field-specific reporting

Please select the one below that is the best fit for your research. If you are not sure, read the appropriate sections before making your selection.

☒ Life sciences   ☐ Behavioural & social sciences   ☐ Ecological, evolutionary & environmental sciences

For a reference copy of the document with all sections, see nature.com/documents/nr-reporting-summary-flat.pdf

Life sciences study design

All studies must disclose on these points even when the disclosure is negative.

Sample size	No statistical method has been used to predetermine sample size. The number of particles used for cryo-EM reconstructions has been indicated in the Extended Data Fig. 4-6.
Data exclusions	Cryo-EM particle exclusion has been performed following standard procedures in the cryoSPARC and Relion softwares. No other data was excluded.
Replication	Experiments were typically repeated in duplicates or triplicates independently to validate the conclusions. The experiment replicate numbers were described in the respective figure legends. All attempts at replication were successful.
Randomization	Not applicable since no groups to be allocated.
Blinding	Not applicable since no groups to be allocated.

Reporting for specific materials, systems and methods

We require information from authors about some types of materials, experimental systems and methods used in many studies. Here, indicate whether each material, system or method listed is relevant to your study. If you are not sure if a list item applies to your research, read the appropriate section before selecting a response.

Materials & experimental systems

n/a	Involved in the study
☐	☒ Antibodies
☐	☒ Eukaryotic cell lines
☒	☐ Palaeontology and archaeology
☒	☐ Animals and other organisms
☒	☐ Clinical data
☒	☐ Dual use research of concern

Methods

n/a	Involved in the study
☒	☐ ChIP-seq
☐	☒ Flow cytometry
☒	☐ MRI-based neuroimaging

Antibodies

Antibodies used	The following commercial antibodies have been used in this study: anti-FcμR mAb (HM14, BD Biosciences), antibody against the strep tag(HuaxingBio, HX1816), his tag (TransGen Biotech, HT501),flag tag(SIGMA, F3165), and HA tag(SIGMA, H3663), goat Anti-mouse IgG HRP (TransGen Biotech, HS201-01). The anti-CD20 IgM antibody was made in our lab, as described in Ref. 43.
Validation	The commercial antibodies were validated by the manufacture, and the following validation statements can be found on the manufacture's website: -Anti-FcμR mAb (HM14) recognizes the levels of human IgM Fc receptor. Species Reactivity: Human (QC Testing). Applications: Flow cytometry (Routinely Tested) -Anti-Strep Tag Mouse Monoclonal Antibody can recognize Strep tag fusion proteins. Species Cross-Reactivity: N/A. Applications: WB. Anti-His Tag Mouse Monoclonal Antibody can recognize 6×His tag fusion proteins. Species Cross-Reactivity: N/ A. Applications: WB, ELISA, IF, IP. -Monoclonal ANTI-FLAG® M2 binds to FLAG fusion proteins. Specificity: Monoclonal ANTI-FLAG® M2 detects a single band of protein on a Western blot from an E. coli crude cell lysate. Species Cross-Reactivity: N/A. Applications: WB, IP, IF. -Anti-HA Tag Mouse Monoclonal Antibody recognizes an epitope located within the sequence YPYDVPDYA (residues 98-106) of the human influenza virus hemagglutinin, known as the HA tag. The product is reactive with HA-tagged fusion proteins expressed at either the amino or the carboxy terminus of the fusion protein. Species Cross-Reactivity: N/A. Applications include WB, ELISA, IF, IP. -Goat Anti-mouse IgG HRP recognizes mouse IgG (H+L). Species Cross-Reactivity: N/A. Applications: WB, ELISA. Validation of the anti-CD20 IgM antibody was carried out using the complement-dependent cytotoxicity assay, as described in Ref. 43.

Eukaryotic cell lines

Policy information about cell lines and Sex and Gender in Research

Cell line source(s)	Sf21, High Five, HEK293F, HEK293T, HeLa cells were originally purchased from ATCC. Jurkat cell, originally purchased from ATCC, was kindly provided by Prof. Jiazhi Hu (Peking University).
Authentication	The cell lines were not authenticated.
Mycoplasma contamination	The cells were regularly tested for free of Mycoplasma contamination by standard PCR method.
Commonly misidentified lines (See ICLAC register)	No commonly misidentified lines were used.

Flow Cytometry

Plots

Confirm that:

☒ The axis labels state the marker and fluorochrome used (e.g. CD4-FITC).

☒ The axis scales are clearly visible. Include numbers along axes only for bottom left plot of group (a 'group' is an analysis of identical markers).

☒ All plots are contour plots with outliers or pseudocolor plots.

☒ A numerical value for number of cells or percentage (with statistics) is provided.

Methodology

Sample preparation	Flow cytometric analyses of cell surface levels of FcμR were performed using the PE-labeled anti-FcμR mAb (HM14, BD Biosciences). To examine IgM binding, cells were incubated with twin-strep tagged Fcμ-J complex at a concentration of 15 μg/mL for 30 min on ice, washed, and then incubated with PE-labeled streptavidin.
Instrument	BD FACS Aria III cell sorter, CytoFlEX S system (Beckman Coulter)

Software	FlowJo (vx.0.7) and GraphPad Prism (v8.0.2).
Cell population abundance	The abundance of relevant cell population was determined based on expression of GFP. The purity of the sort was >90% as confirmed by expression of GFP in post-sort sample. In analyses of cell surface levels of FcμR and binding, approximately 20,000 cellular events were collected for each sample. Frequencies of cell populations are indicated on the flow plots in the supplementary information.
Gating strategy	Cells were first gated on FSC-A/SSC-A plots to exclude dead cells and debris. FSC-A/FSC-H and SSC-A/SSC-H plots were then used to determine singlet gates. Positive populations were determined by adjusting the threshold of the gate to the unstained samples. Gating strategy is shown in the Extended Data.

☒ Tick this box to confirm that a figure exemplifying the gating strategy is provided in the Supplementary Information.